SECTION A

Section A has been submitted to and received by the Australian Journal of Earth Sciences

A REVISED DEFORMATION CHRONOLOGY FOR THE BENDIGO GOLDFIELD, CENTRAL VICTORIA, AUSTRALIA: THE IMPORTANCE OF POST D_2 DEFORMATION EVENTS

Abstract

The structural evolution of the Bendigo Goldfield, Victoria, Australia, involves four stages of deformation (D_1-D_4). D_1 is defined by a penetrative foliation (S_1) that is parallel to sub-parallel with bedding (S_0), folded around F_2 folds and crenulated by an axial planar fabric (S_2). D_3, as defined in this study, was previously unrecognised and is characterised by four sets of conjugate kink bands that overprint and deform F_2 and S_2. The D_3 kink bands possess extensional geometry and are arranged in orthorhombic symmetry about a sub-vertical axis. It is suggested that the geometry of kilometric-scale D_3 kinks could, in part, explain the outcrop pattern observed at Bendigo and more significantly, the domal culminations that are associated with the localisation of gold. D_4 is defined by a non-penetrative, west-striking foliation (S_4) characterised by contractional kink bands. D_1 and D_2 clearly indicate distinct, yet progressive phases of ENE-WSW shortening within the one orogeny (Benambran?). D_3 could represent the later stages of the Benambran Orogeny or part of the younger Tabberabberan Orogeny. N-S shortening during D_4 indicates that a rotation of the principal shortening axis has occurred and as such, D_4 may correspond to the later stages of the Tabberabberan Orogeny.

Key words: Bendigo Goldfield, central Victorian goldfields, deformation history, kink bands.

INTRODUCTION

The Bendigo Goldfield is the largest goldfield within the Lachlan Fold Belt of eastern Australia (Figure 1a) and is a classic example of a structurally controlled, turbidite-hosted gold deposit. Globally, similar deposits occur within the Meguma terrane, Nova Scotia (Ryan & Smith, 1998), the Otago Schist, New Zealand (Smith *et al*. 1996) and the Juneau terrane, Alaska (Goldfarb *et al*. 1986). This style of deposit is characterised by multiple phases of deformation and structural overprinting, which can make it difficult to evaluate in-situ mineralisation.

The structural chronology preserved in the host rock at Bendigo is a contentious issue, with as many as three stages of deformation being proposed (Forde, 1989; Schaubs & Wilson, 2002). Early workers (e.g. Stone, 1937; Chace, 1949) make reference to the possibility that gold deposition may have occurred after the main phase of quartz vein emplacement. Despite such interpretations, the concept of polyphase deformation at Bendigo has largely been ignored and may be one of the fundamental reasons why the

distribution of gold, particular in three-dimensions, is poorly understood and frequently reported as being erratic (e.g. Dominy & Johansen, 2004).

Since 1993, Bendigo Mining Ltd. has been re-evaluating and re-developing part of the goldfield. The new development accesses eight auriferous reefs to a depth of ~800 m and offers a unique opportunity to re-examine the structurally controlled auriferous reefs, which characterise the central Victorian goldfields (c.f. Cox *et al*., 1991a). This study identifies several tectonic foliations, visible both proximal and distal to the mineralisation. The presence of multiple foliations, which post-date D_2, suggests that the deformation history is more complex than previously thought. The aim of this paper is to document post-D_2 foliations and produce a revised structural chronology for the Bendigo Goldfield.

GEOLOGICAL SETTING

The Bendigo Goldfield is located within the state of Victoria, Australia, approximately 130 km northwest of Melbourne (Figure 1a, b). The geology of Victoria is dominated by the Lachlan Fold Belt (LFB; Figure 1a; Glen, 1992; Gray & Foster, 1998), which forms part of the Palaeozoic Tasman Fold Belt of eastern Australia (Figure 1a; Ramsay & VandenBerg, 1986; VandenBerg *et al*., 2000). Geologically the LFB can be subdivided into western, central and eastern sub-provinces (Figure 1a; Gray *et al*., 1997). The Western Sub-province (WSP; Figure 1a) consists of three fault-defined structural zones (Stawell, Bendigo and Melbourne; Gray, 2003) and is dominated by a monotonous succession of deformed and metamorphosed Cambro-Ordovician to Silurian turbidites. The metasediments are typical of medium-*P/T* (Barrovian type) conditions and predominantly exhibit prehnite-pumpellyite facies metamorphism (Offler *et al*., 1998). The interzone faults that separate the Stawell, Bendigo and Melbourne Zones are major strike parallel, west-dipping thrust faults (Gray & Foster, 1998), which have a listric geometry (Gray & Willman, 1991a, b; Gray *et al*., 1991). These thrusts probably feed into a detachment at depth, situated either at the Ordovician Cambrian boundary or deeper within the Cambrian basement (Cox *et al*., 1991a, b; Gray *et al*., 1991; Gray & Willman, 1991a).

The principal style of deformation observed across the WSP has been attributed to a thin-skinned style of crustal shortening, with the formation of a predominantly east-vergent, N-S to NW-SE striking, fold and thrust belt (Gray & Willman, 1991a, b, c; Cox

et al., 1991b). The total amount of ~E-W shortening attributed to folding, reverse faulting and cleavage development has been estimated to be in the order of 50 to 70% for the Stawell Zone and Bendigo Zone (Cox *et al*., 1991a; Gray & Willman, 1991a, c), and 30 to 50% for the Melbourne Zone (Gray & Willman, 1991a).

Geochronological research by Foster *et al*. (1998) demonstrates that metamorphism and deformation was diachronous from west to east across the WSP, beginning in the Late Ordovician-Early Silurian (Stawell and Bendigo Zones) through to Late Silurian-Early Devonian (Melbourne Zone). Foster *et al*. (1998) conclude that the fold and thrust belt of the WSP formed as a result of an eastward-migrating deformation front during the Silurian to Early Devonian, and therefore most orogenic activity actually took place before the Tabberabberan Orogeny. These findings, which are in general agreement with others (e.g. Collins & Vernon, 1992; Arne *et al*., 1998; Ramsay *et al*., 1998) rule out a synchronous, province-wide mineralising event and instead suggest that mineralisation was episodic and associated with both regional metamorphism and the later stages of deformation.

Structural research carried out within the Western Sub-province, the Eastern Sub-province and north-eastern Tasmania suggests episodic and progressive deformation involving substantial ~E-W shortening (e.g. Powell & Rickard, 1985; Wilson & de Hedouville, 1985; Watchorn & Wilson, 1989; Forde, 1989; Wilson *et al.,* 1992; Powell & Baillie, 1992; Miller & Gray, 1996; Miller *et al*., 2001; Schaubs & Wilson, 2002). A later period of ~N-S shortening is observed across the LFB and overprints the prominent N-S to NW-SE structural grain (e.g. Powell *et al*., 1985; Stubley, 1990; Forde, 1989; Glen, 1992; Wilson *et al.,* 1992; Forde & Bell, 1994; Goscombe, *et al*., 1994, Gao *et al*., 1995; Morand *et al*., 1997; Miller *et al*., 2001; Miller & Wilson, 2002, 2004).

Dyke swarms and felsic to intermediate intrusions with S- and I-type affinities were emplaced during two broad intervals. The first, between 410-390 Ma (Early Devonian) occurred primarily across the Stawell Zone and western part of the Bendigo Zone, whilst the second, between 380-360 Ma (Mid to Late Devonian) occurred across the Bendigo and Melbourne Zones (Foster *et al*., 1998). A younger period of lamprophyre dyke emplacement has been dated at 155 Ma (Jurassic) by McDougall & Wellman (1976).

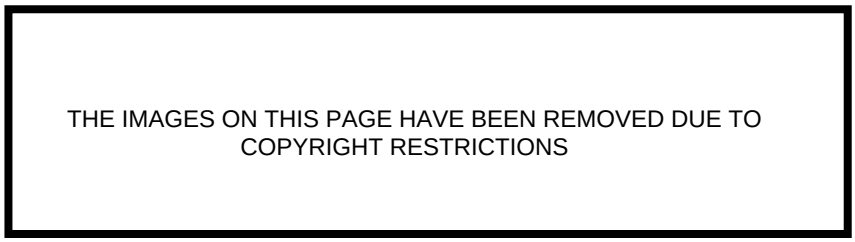

Figure 1. *A. The Lachlan Fold Belt in mainland Australia (LFB). Adapted from Gray* et al. *(1997). B. The location of Bendigo within the Bendigo Zone (BZ). Adapted from Gray and Willman (1991a). C. Geological map of the Bendigo region, showing biostratigraphic units, intra-zone faults and the Bendigo Goldfield. Adapted from Johansen (2001). D. Map of Bendigo, showing the locality of sites studied. Current underground mine development extends northward from the Carshalton mine site for approximately 2.5 km and to a depth of 800 m.*

The Bendigo Goldfield is situated within the Bendigo Zone (BZ; Figure 1b) and lies within a 9 km wide NNW trending zone of deformed, Lower to Middle Ordovician turbiditic metasediments bound by the intrazone, west-dipping Whitelaw and Sebastian thrust faults to the east and west respectively (Figure 1c). The Ordovician metasediments, which typify the Bendigo region, exhibit rapid and distinct facies changes and belong to a succession of sandstones, siltstones, shales, thin polymict conglomerates and minor cone-in-cone limestones known as the Castlemaine Supergroup (Cas & VandenBerg, 1988). Based on graptolite assemblages found principally within the shale units, the Castlemaine Supergroup has been subdivided into six biostratigraphic units (Figure 1c).

The mineralisation at Bendigo (Dunn, 1896; Whitelaw, 1914; Stone, 1937; Chace, 1949; Mckinstry & Ohle, 1949; Thomas, 1953b; Sharpe & MacGeehan, 1990; Cox *et al*., 1991a; Willman & Wilkinson, 1992; Jessell *et al*., 1994; Turnbull & McDermott, 1998; Jia *et al*., 2000) is intimately related to the structural evolution of the goldfield (e.g. Forde, 1989; Forde & Bell, 1994; Schaubs and Wilson, 2002; Schaubs & Zhao, 2002). However, the structural chronology preserved within the host rock is contentious and therefore unclear.

ANALYTICAL PROCEDURES

Samples and thin sections

Approximately 80 orientated, pelitic to semi-pelitic samples were collected from both on-reef and remote development underground. On surface additional orientated samples were collected from Victoria Hill; the Carshalton mine site; Diamond Hill and Central Drive at La Trobe University (Figure 1d). To ascertain the microstructural history horizontal sections and vertical sections orientated parallel (P section) and normal (N section) to the S_2 foliation (see second deformation stage below) were cut for twelve samples. Analysis of the thin section suites revealed that similar microstructural histories were preserved within each of the samples. The correlation of foliations between different samples was in part ambiguous, due to differences in the relative intensity of the conjugate S_3 foliations (see third deformation stage below). It was therefore not possible to fully resolve the deformation history using only horizontal, P and N sections. To overcome this five orientated samples were selected from different

locations and suites of up to 15 sections cut for each. The thin section suites included a horizontal, N and P section and intermediate sections with dips of 20°, 40° and 60° in the four directions defined by horizontal to N section and horizontal to P section. This number and orientation of thin sections allowed each sample to be analysed in great detail from a three-dimensional perspective.

Orientation measurements and estimated errors

The orientation of a foliation (e.g. S_1) was measured for each thin section in a suite and then plotted on a stereonet as a pitch within the plane of that section, unless the section was horizontal, in which case the orientation was plotted as a bearing. A great circle was constructed as a best fit through the resultant points in order to define the true orientation of that foliation.

The total accumulated error in determining the orientation of the kink bands observed in thin section is estimated as ± 9°. This value consists of errors (± 8°) incurred during the orientation and preparation of hand specimens and thin sections (Bell *et al*., 1997), and a precision error of ± 1° for measurements made from the thin sections.

To ascertain the precision of the orientation measurements 3 thin sections were chosen and 50 orientation measurements taken for each foliation (S_1 to S_4). A vector mean (Mardia, 1972; Fisher, 1993) was calculated for each foliation and then plotted as a running mean against the number of readings (n = 50). This demonstrated that for a single foliation within a section it was necessary to take a minimum of 21 measurements in order to achieve a vector mean with a precision of ±1°. The resultant vector means for a foliation were plotted (as above) and a best-fit great circle constructed to represent the true orientation of that foliation (e.g. Figure 4b & Figure 6b). This process was carried out for each suite of thin sections.

Vector analysis of F_2 axial traces

As part of the third deformation stage (see below) F_3 folds are proposed on the basis of a reinterpretation of the 1:10000 geological maps for the Bendigo Goldfield (Eaglehawk, Golden Square & Spring Gully sheets; Willman & Wilkinson, 1992). In order to quantify the presence of these folds vector analysis has been carried out on the F_2 axial traces (see second deformation stage below), which lie within the goldfield.

Centre points between the digitised nodes of F_2 axial traces (Appendix B, Part 1 & 2) were generated. The orientation of the line which joined the original nodes was assigned to the respective centre point. The vector mean (Mardia, 1972; Fisher, 1993) for the F_2 axial traces (165°) was calculated from the strike of the centre points.

The precise location and extent of F_3 was determined by plotting the data with a dextral or sinistral rotation of F_2 equal to or greater than 9° from 165 ° (Figure 5a, b). The value of 9° was determined from the analysis of extensional kink bands observed in horizontal thin sections (Appendix B, Part 3).

STRUCTURAL CHRONOLOGY

Four overprinting tectonic foliations (S_1-S_4) have been recognised within the Bendigo Goldfield and a four-stage deformation history (D_1-D_4) is proposed. The individual stages of deformation are presented in chronological order, with emphasis placed on D_3 and D_4.

First deformation stage (D_1)

The earliest tectonic foliation recognised by this study (S_1) is a penetrative, mesoscopically visible planar fabric, which is most evident in pelitic and semi-pelitic rocks. In pelites, S_1 is predominantly defined by a strong bedding-parallel to sub-parallel alignment of layer silicates and opaque minerals, whereas in arenaceous units S_1 has a rough morphology, occurring as an elongation of quartz grains with finely crystallised layer silicate films and fibrous quartz-mica beards (Figure 2a, b). In several sections S_1 is oblique to bedding, the best examples of which can be seen when S_1 refracts slightly as it passes from a pelitic to an arenaceous unit (Figure 2a). A relic foliation corresponding to S_1 can be observed within a number of quartz veins (Figure 2c).

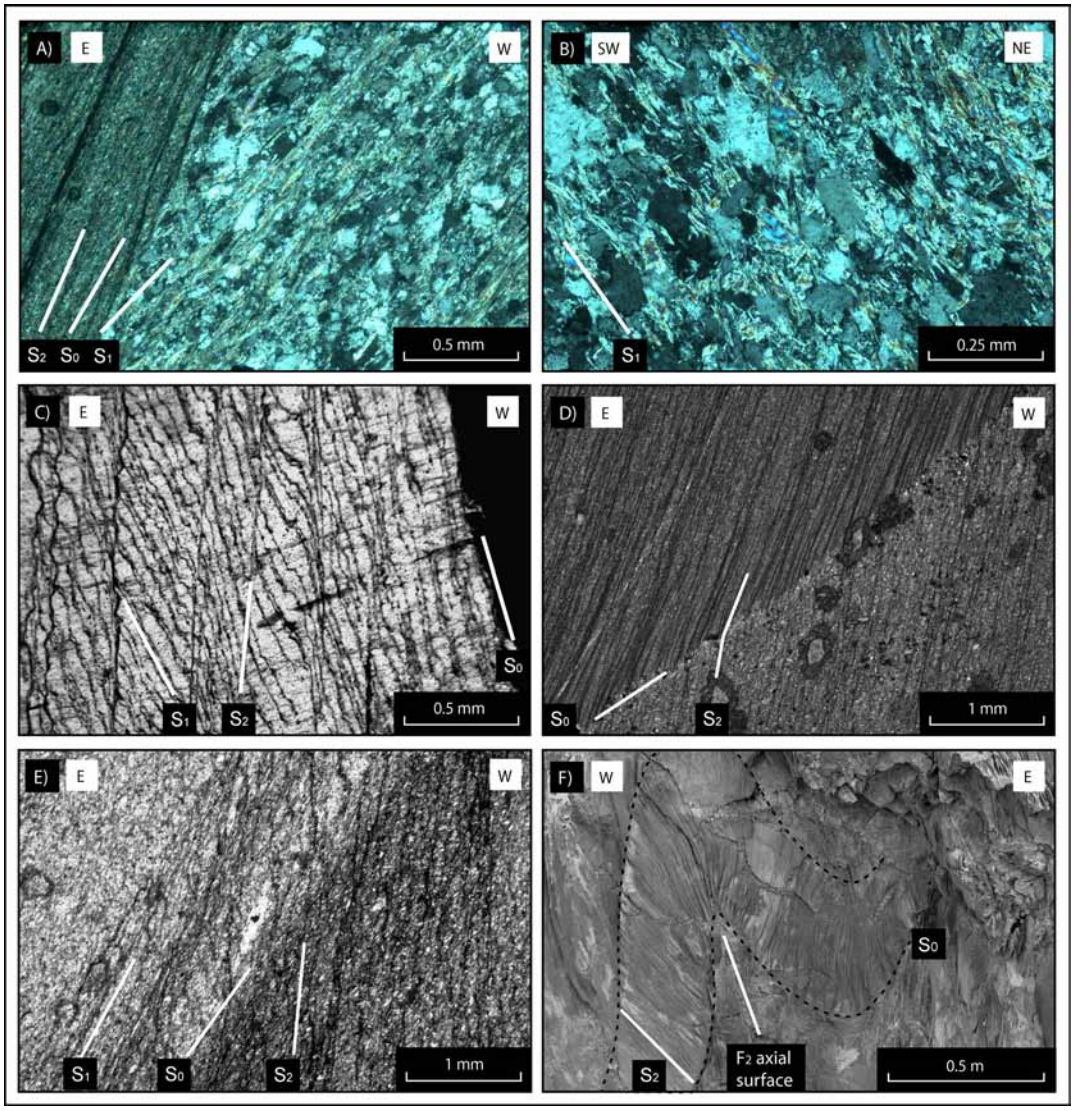

Figure 2. *A. S_1 defined by a strong alignment of layer-silicates oblique to S_0. XPL. Thin-section dips at 90° towards 007°. Sample GT1v. B. S_1 exhibiting a rough morphology with elongate quartz grains, finely crystallised layer silicate films and quartz-mica beards. XPL. Thin-section dips at 90° towards 155°. Sample G131a. C. S_1 and S_2 preserved within replacement quartz. PPL. Thin-section dips at 90° towards 158°. Sample D3X014a. D. S_2 exhibiting a divergent fanning geometry within a pelitic unit. PPL. Thin-section dips at 90° towards 351°. Sample S3 111. E. S_2 truncates S_0 and S_1, and is refracted by a change in lithology. PPL. Thin-section dips at 90° towards 340°. Sample C118v. F. S_2 occurring as a differentiated solution cleavage with a convergent fanning geometry. New Chum Anticline, Eaglehawk, Bendigo.*

The first phase of deformation resulted in the initiation of the regionally extensive ~N-S striking thrust belt, with the development of first and second order faults. Interzone faults such as the Avoca and Heathcote faults (Figure 1b) are examples of first order faults, whereas intrazone faults such as the Whitelaw and Sebastian faults (Figure 1c) are examples of second order faults. At Bendigo ~1500 m of vertical displacement has been associated with the intrazone Whitelaw fault as indicated by biostratigraphic zonation, which showed the juxtaposition of Lancefieldian and Darriwilian rocks (Harris, 1934).

Bedding-parallel, laminated quartz veins (LQVs; Dunn, 1896; Chace, 1949; McKinstry & Ohle, 1949; Forde, 1989; Jessell *et al*., 1994; Fowler, 1996) observed at Bendigo also formed early in the deformation history. The LQVs predate D_2 because they are deformed by S_2 and folded around F_2, with parasitic folding present within a number of F_2 hinges (see Plate 14 in Willman & Wilkinson, 1992; Gray & Willman, 1991c). The laminated veins formed predominantly by replacement (McKinstry & Ohle, 1949; Chace, 1949; Forde, 1989) during a period of layer-parallel shearing (D_1).

Second Deformation Stage (D_2)

The most intense foliation recognised by this study (S_2) is a well-developed, axial planar crenulation cleavage (Figure 2d, e, f). In pelitic units S_2 is a closely spaced, penetrative cleavage that occurs as a slaty cleavage with a divergent fanning geometry in higher strain zones (Figure 2d). S_2 in pelites is characterised by a differentiated layering of layer silicate rich domains and quartz rich domains. In arenaceous units S_2 is best developed within F_2 hinge zones, where it occurs as a spaced, differentiated solution cleavage with a convergent fanning geometry (Figure 2f).

First order D_2 folds consist of regional anticlinoria and synclinoria with wavelengths of 3-15 km and amplitudes in the order of 1-2 km (Thomas, 1939; Gray & Willman, 1991a, c). At Bendigo, second order folds (here referred to as F_2) are tight, essentially upright chevron folds characterised by their regular frequency and persistence along strike. F_2 exhibit average wavelengths of between 300 to 400 m, amplitudes of between 150 to 300 m and interlimb angles of between 20° and 50° (Willman & Wilkinson, 1992; Johansen, 2001). Localised changes in F_2 fold plunge, with plunges of up to 60° observed (Dunn, 1896; Whitelaw, 1914), occur across the Bendigo Goldfield and give rise to smaller scale dome and basin structures (e.g. Stone, 1937).

At least three orders of faults were active across the WSP during D_2. First and second order faults include the Heathcote fault and Whitelaw fault respectively (Gray & Willman, 1991c), whereas deposit scale reverse faults represent the third order of faults. At Bendigo third order D_2 faults display geometries that are influenced by folding (Figure 3). In places the faults truncate F_2 and S_2, which implies that they formed during the later stages of fold amplification and tightening. The third order faults were active during D_2 quartz veining with subsequent reactivation occurring during D_3 and D_4.

The majority of the quartz veining observed at Bendigo was emplaced during the latter part of D_2. Quartz bodies occur in the simplified form of: (1) saddle, trough and leg reefs; (2) neck reefs; (3) fault reefs; (4) spur reefs; (5) laminated veins; (6) breccia veins; and (7) cross-course reefs (see Forde, 1989; Sharpe & MacGeehan, 1990; Cox *et al*., 1991a, 1995; Johansen, 2001; Schaubs & Wilson, 2002; and references therein). The D_2 reefs and veins have been reactivated by later phase(s) of deformation and crosscut by later vein generations.

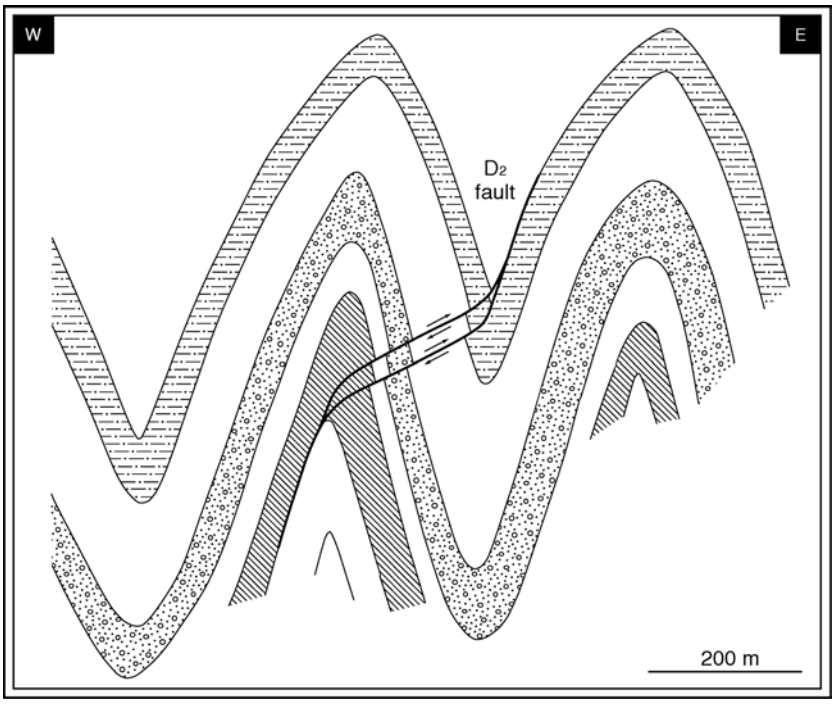

Figure 3. *A simplified geometry for third order D_2 faults. The D_2 faults become discordant once they pass through the fold axial surface. At this point the faults commonly flatten slightly and bifurcate, before rejoining and returning to a bedding-parallel orientation on the limb of an adjacent F_2 fold.*

Third Deformation Stage (D_3)

The third deformation stage recognised by this study is characterised by well-developed extensional kink bands (sensu Ramsay & Huber, 1987; Figure 4a). The D_3 kink bands vary in size from a planar fabric (S_3) on a millimetre scale, through to large-scale kinks (here referred to as F_3) with widths of hundreds of metres and strike lengths of kilometres.

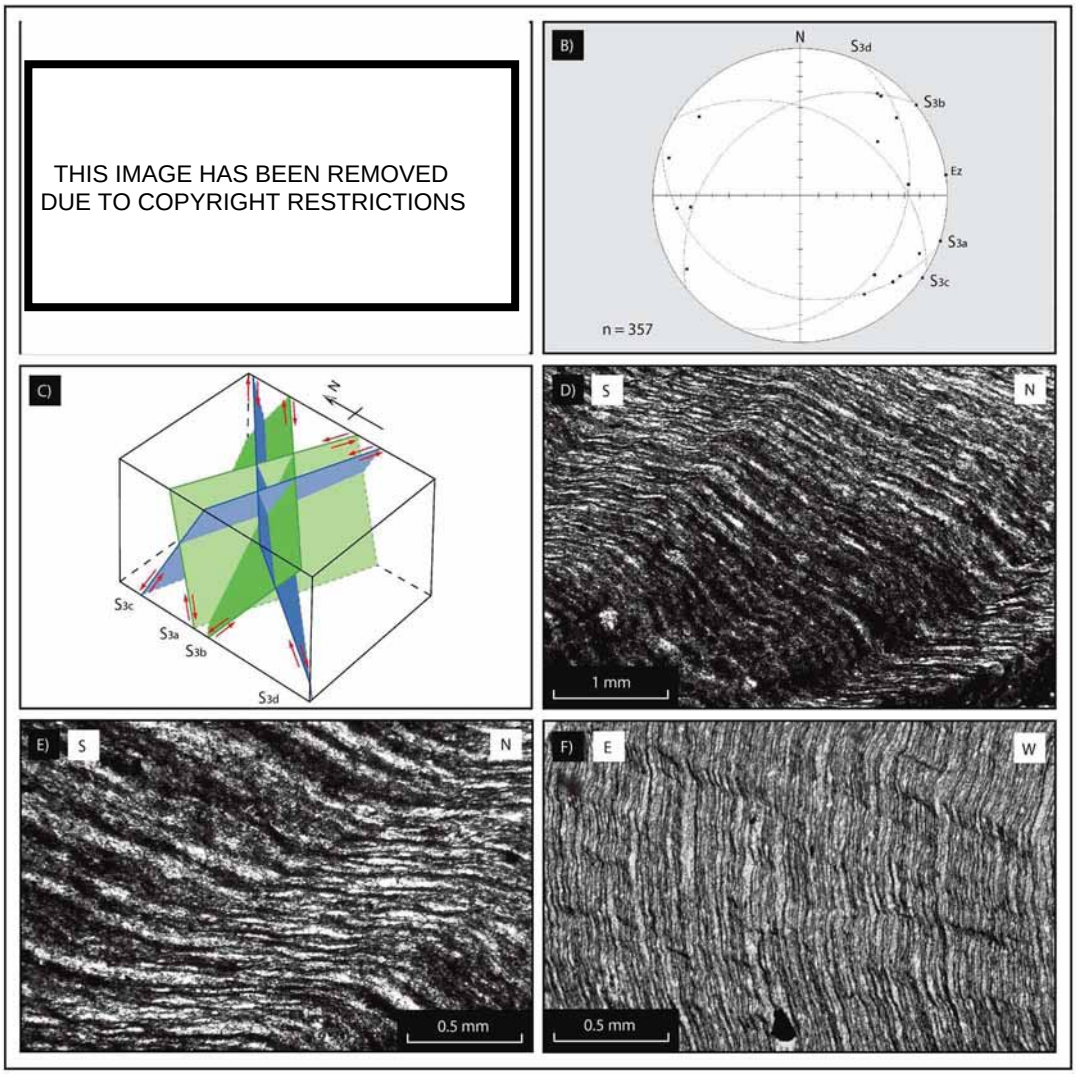

***Figure** 4. S_3 foliation. A. Idealised geometry of extensional kink bands. Modified from Ramsay and Huber (1987). B. Stereonet showing the orientations of the four S_3 foliations within one suite of 15 thin sections. The inferred principal shortening direction (ε_z) is shown. C. Simplified 3-D model showing the orientation of the S_3 foliations. D & E. Extensional S_3 kink bands. PPL. Thin-section dips at 20'towards 0849 Sample G134. F. S_3 crenulations and kznk bands. PPL. Thin-section dips at 90° towards 354°. Sample G134.*

S_3 consists of four coeval sets of well-developed, non-penetrative kinks and crenulations that deform S_2 and lie in orthorhombic symmetry about a sub-vertical axis (Figure 4b, c). In thin section the conjugate kink bands are generally characterised by slightly rounded hinges, planar to curved limbs and planar axial surfaces (Figure 4d, e, f). The mean orientations of the kink band axial surfaces and their respective shear senses are presented in Table 1. The D_3 principal shortening direction for the kink bands trends ~081° (Figure 4b) and was determined using the conjugate bisector method of Ramsay (1962).

Table 1. *Mean orientations for D_3 kink band axial surfaces and respective shear senses.*

Foliation	Strike	Dip	Shear sense
S_{3a}	WNW	50-55°	Sinistral
S_{3b}	NE	60-65°	Dextral
S_{3c}	ESE	50-55°	Sinistral
S_{3d}	SW	55-60°	Dextral

Thin section analysis and the identification of L_3^2 intersection lineations has shown that S_3 is present throughout the goldfield and current mine development, occurring not only in close proximity to mineralisation but also on F_2 limbs, well away from the influence of structures such as faults.

Distinct changes in F_2 plunge and the strike of S_0, S_1 and S_2 define the F_3 kink band axial surfaces (Figure 5a, b, c). The plunge of F_2 within F_3 is variable, with plunges in excess of 30° observed in a number of localities. Perpendicular to the strike of F_3, changes in S_3 intensity are often rapid, defining zones of high strain within F_3. External to F_3, S_3 is weak and rarely observed. High strain zones vary in width from a few metres up to tens of metres, however, their full extent along strike and down dip remains unclear due to a lack of continuous exposure.

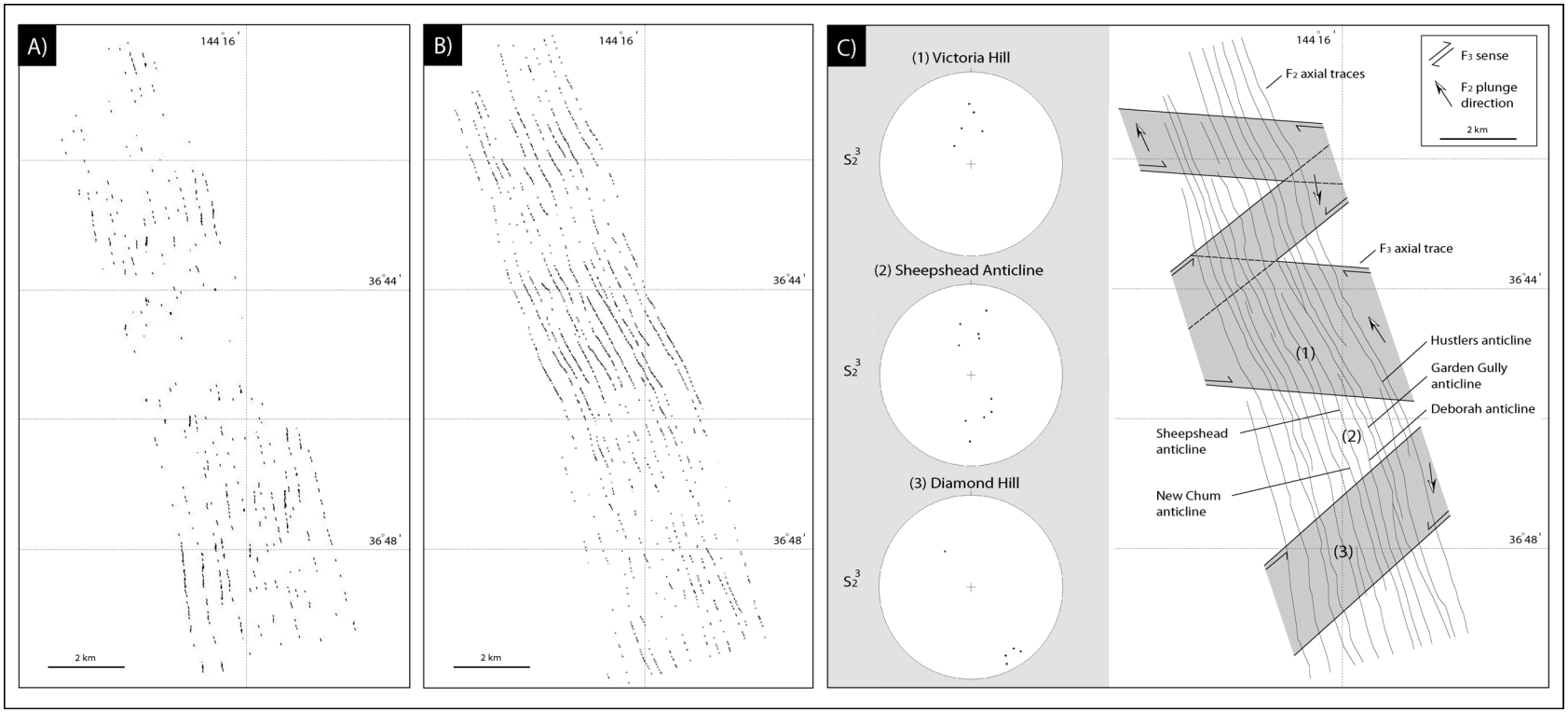

Figure 5. *A. Plot of centre points where each point represents a dextral rotation in the strike of F_2 equal to or greater than 9° from the vector mean (165°). B. Plot of centre points where each point represents a sinistral rotation in the strike of F_2 equal to or greater than 9° from the vector mean (165°). C. F_2 axial traces within the Bendigo Goldfield. Large-scale uniform rotations (F_3) in the strike of F_2 are highlighted in grey and were deduced form the reinterpretation of geological maps and vector analysis. The general plunge direction of F_2 within F_3 is shown (see Figure 7). The subtle nature of the kinks is due primarily to the oblique intersection of F_3 with the current topography. Stereonets show the plunge and plunge direction of L_2^3 intersections from three localities within the goldfield. These localities are up to ~5km apart and highlight the goldfield extent of S_3.*

D_3 faults

Progressive E-W shortening during D_3 produced oblique faults, which crosscut the prominent NNW-SSE structural trend. Within the goldfield such faults have been termed "crosscourses" (Stone, 1937; Chace, 1949). Gray & Willman (1991c) and Willman & Wilkinson (1992) identify two sets of conjugate oblique faults, the first trends WNW (110°-125°) and has a sinistral horizontal separation, whilst the second set trends NNE (010°-035°) and has a dextral horizontal separation. A principal shortening direction trending 4°/250° is proposed for the conjugate faults by Gray & Willman (1991c) and Willman & Wilkinson (1992). The orientation of the oblique faults is comparable to the D_3 kink bands. Figure 9 in Willman & Wilkinson (1992) shows two strike parallel oblique faults with opposing dip directions, the same geometry displayed by S_{3b} and S_{3d} (Figure 4b, c). Ruptured kink band axial surfaces are commonly observed in thin section, which may suggest that on a larger scale D_3 faults developed along F_3 axial surfaces.

Fourth Deformation Stage (D_4)

The fourth deformation stage recognised by this study is characterised by well-developed contractional kink bands (*sensu* Ramsay & Huber, 1987; Figure 6a, b). D_4 kinks vary in size from a planar fabric (S_4; Figure 6c, d, e) through to larger scale kinks (here referred to as F_4) with widths of up to a metre and strike lengths of tens of metres (Figure 6f). The S_4 foliation consists of non-penetrative crenulations and kink bands, which deform S_3 (Figure 6c). D_4 kink bands are best developed in pelitic to semi-pelitic sequences and generally display rounded hinges, curved limbs and planar axial surfaces (Figure 6c, d, e). Kinks are not observed within arenite-dominated sequences, which suggests that the more competent units prevented the nucleation and propagation of kink bands. The D_4 kinks have a dextral shear sense and axial surfaces that dip at ~52° towards ~180° (e.g. Figure 6b). Based on the geometry of the kink bands the principal shortening direction during D_4 was ~N-S and the principal extension direction ~E-W.

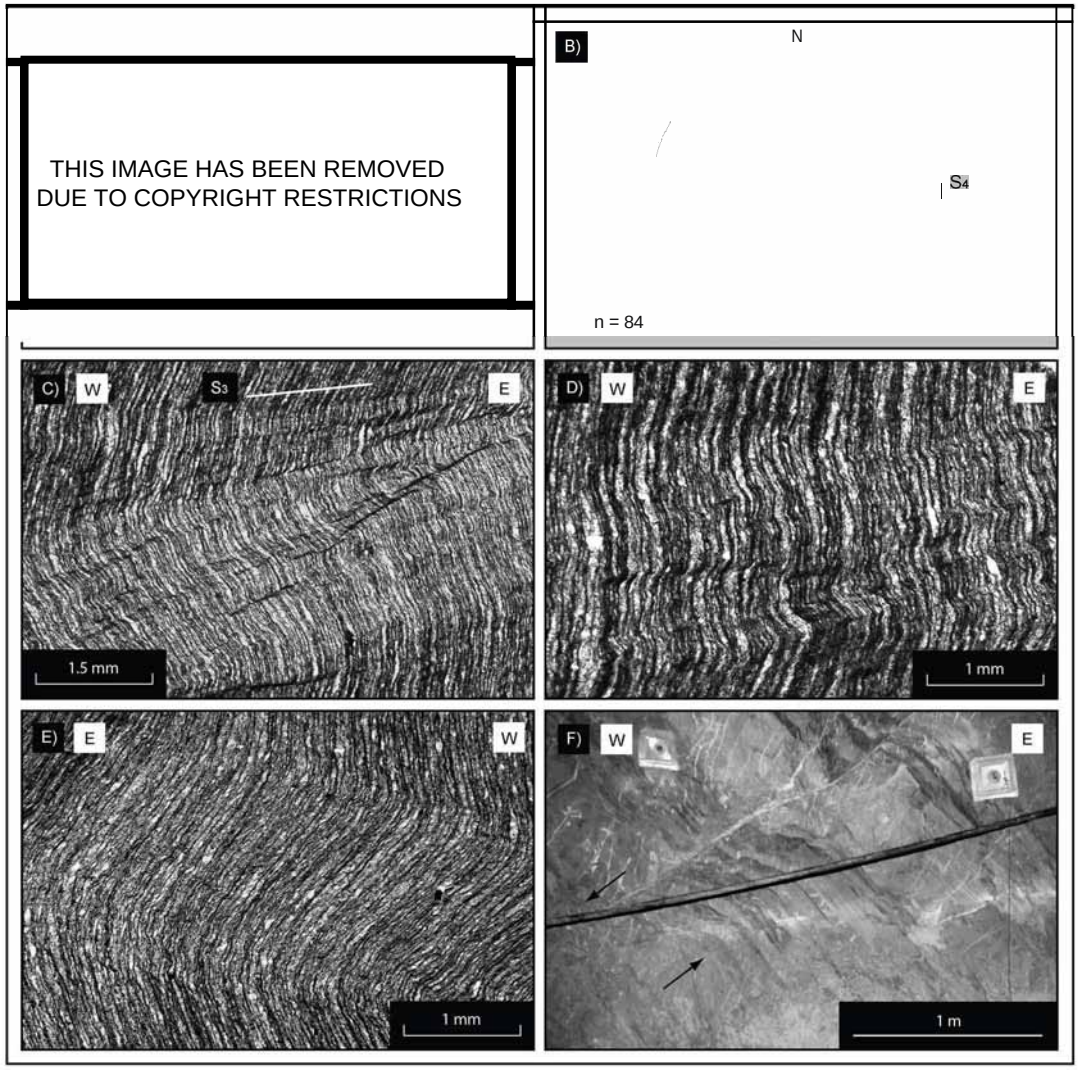

Figure 6. *S_4 foliation. A. Idealised geometry of contractional kink bands. Modified from Ramsay and Huber (1987). B. Stereonet showing the orientation of the S_4 foliation within one suite of thin sections. C. Small-scale contractional kink bands (S_4) deforming S_2 (sub-vertical) and S_3 (sub-horizontal). PPL. Thin-section dips at 90° towards 174°. Sample G134. D. Small-scale contractional kink band that deforms S_2 (sub-vertical) and exhibits a complex internal structure. PPL. Thin-section dips at 90° towards 174°. Sample G134. E. A well-developed small-scale contractional kink band that deforms S_2 (sub-vertical) and exhibits slightly rounded hinge zones. PPL. Thin-section dips at 90° towards 354°. Sample G134. F. Metre-scale contractional kink band (F_4). Upper axial surface has ruptured with quartz veining present in zones of dilation.*

D_4 faults?

Normal faults crosscut the prominent NNW-SSE structural trend (Figure 7) and formed late in the structural development of the goldfield. The normal faults have dextral sense and orientations comparable to D_4 kinks, which is indicative of E-W extension (Figure 7). It is possible that at least some of these faults are reactivated D_3 oblique faults with a reversed shear sense.

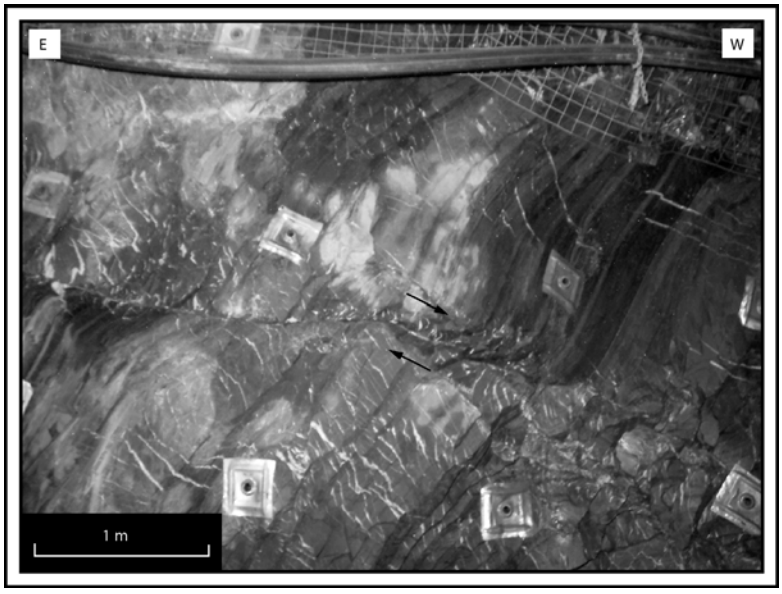

Figure 7. *D_4 normal fault and minor en echelon quartz veining. Access development, Young's Reef.*

At least two generations of strike-slip associated slickenlines have been observed on a number of D_2 fault planes (Figure 8a, b). A single generation of sub-horizontal slickenlines can also be observed on Jurassic lamprophyre dykes (e.g. at Victoria Hill), which crosscut D_4 structures. The sub-horizontal slickenlines postdate the lamprophyre dykes because firstly, the slickenlines are preserved along thin sheets of carbonate on the dyke walls and secondly, several D_2 faults have been reactivated post dyke emplacement (Figure 8c, d). It is most likely that the first generation of slickenlines (marked 'A' in Figure 8b) formed during D_4 and that the second generation (marked 'B' in Figure 8b) formed as a result of sub-horizontal displacement, which occurred after dyke emplacement.

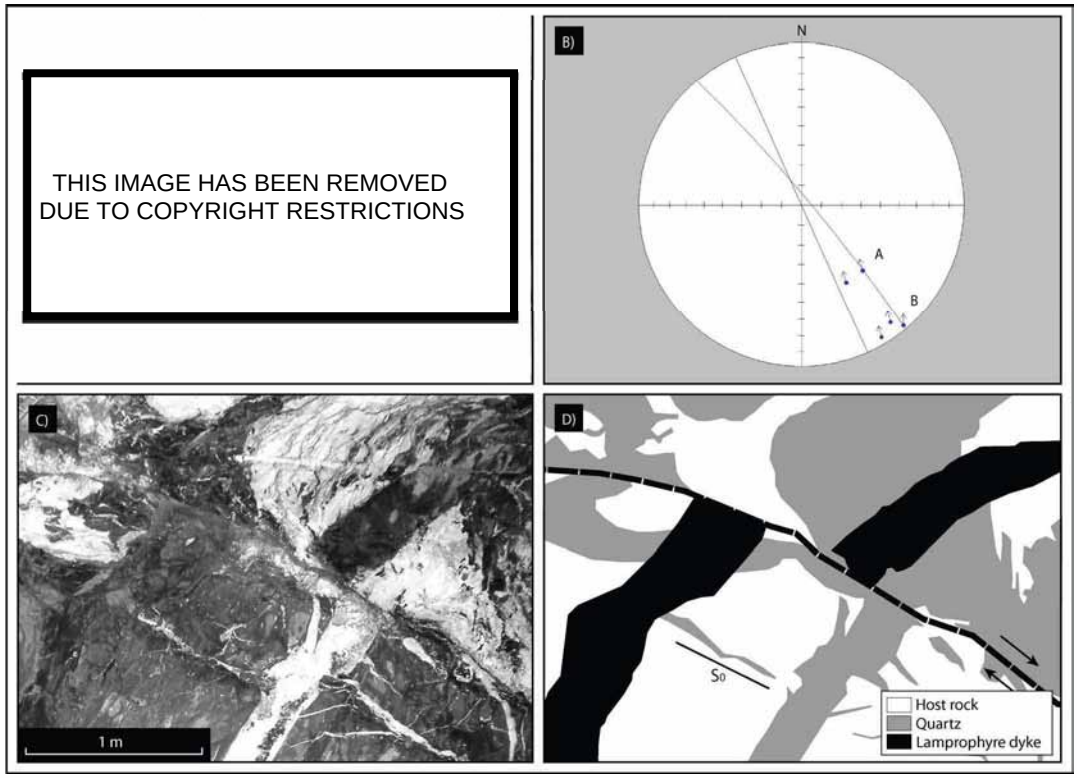

Figure 8. *A. View to the north of a fault controlled auriferous reef. Visible gold indicated by pink dots. Late stage strike-slip reactivation of the hangingwall fault plane has truncated gold bearing structures (e.g. stylolites). Photograph courtesy of Bendigo Mining Ltd. B. Stereonet showing the orientation of slickenlines associated with late-stage strike-slip reactivation of the fault. The sub-horizontal slickenlines (marked 'B') are the younger. The sense on both sets of slickenlines is east side up and sinistral. C & D. View to the south of a D_2 fault reactivatedpost dyke emplacement, sense of movement is hangingwall to the south-southwest. Upper S3 Reef, Sheepshead anticline.*

DISCUSSION

D_1 signifies the onset of ~E-W shortening (Table 2) and possibly the beginning of the Benambran Orogeny (VandenBerg *et al.*, 2000). At Bendigo D_1 involved the initial formation of the Sebastian and Whitelaw thrust faults and the development of a bedding parallel to sub-parallel tectonic foliation (S_1). The S_1 foliation recognised by this study is considered to be equivalent to the bedding-parallel fabrics of Williams, (1972) and Cox *et al.*, (1991b), the $S_{1/2}$ cleavage of Powell, (1983), the S* cleavages of Powell & Rickard, (1985) and Wilson & de Hedouville, (1985), the S_1 cleavages of Forde, (1989), Wilson *et al.*, (1992) and Forde & Bell, (1994) and the $S_\circ$ cleavage of Schaubs & Wilson, (2002). Although numerous authors have recognised the presence of an early

fabric within the LFB, the origin of this fabric is subject to debate. The S_1 foliation observed within the Bendigo Goldfield clearly truncates bedding in a number of thin sections. In agreement with Wilson & de Hedouville, (1985), Wilson *et al*., (1992), Forde & Bell (1994), S_1 is considered to have formed in response to an early phase of layer-parallel shearing, thrust faulting and low grade metamorphism, which occurred prior to the development of the first mesoscopic folds (F_2).

Table 2. *Summary of the four-stage deformation chronology proposed for the Bendigo Goldfield.*

Deformation stage	Principal extension directions ($\varepsilon_1>\varepsilon_2>\varepsilon_3$)	Primary structures
D_4	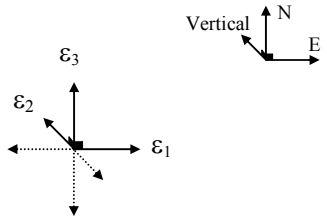	Contractional kink bands Normal faults & shear zones
D_3	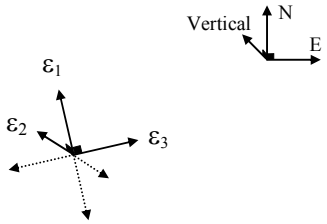	Conjugate extensional kink bands Oblique faults
D_2	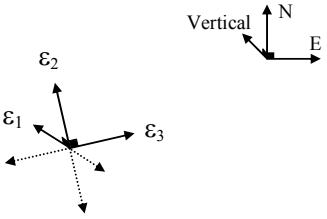	Mesoscopic chevron folds Axial planar crenulation cleavage Deposit scale reverse faults Major quartz reefs
D_1	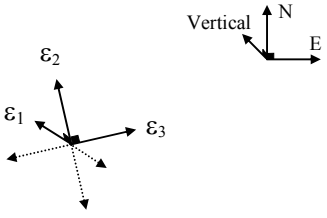	Inter- & intra-zone thrust faults Sub-horizontal tectonic foliation Laminated quartz veins (LQVs)

D_2 represents progressive deformation and is the most intense period of deformation recognised at Bendigo. In context with the models of VandenBerg *et al*. (2000) D_2 is considered to represent the peak of deformation and metamorphism during the Benambran Orogeny. D_2 is characterised by the formation of the first generation of mesoscopic folds and associated axial planar cleavage (S_2). The axial planar S_2 foliation is widely recognised across the LFB (e.g. Williams, 1972; Forde, 1989; Cox *et al*, 1991b; Gray & Willman, 1991c; Wilson *et al*., 1992; Goscombe *et al*., 1994; Schaubs & Wilson, 2002). The predominant NNW-SSE trend of F_2 and S_2 implies that the direction of maximum shortening during D_2, like D_1, was approximately ENE-WSW. The geometry of F_2 and D_2 faults (Figure 3) indicates that the direction of maximum extension was vertical (Table 2).

D_3 was previously unrecognised at Bendigo and represents renewed ENE-WSW shortening and the deformation of F_2 and S_2 (Table 2). D_3 structures include conjugate extensional kink bands and oblique faults (Figure 4d, e, f). The D_3 kink bands vary in size from a planar fabric (S_3) on a millimetre scale (e.g. Figure 4d) through to large-scale kinks (F_3) on a kilometre scale (Figure 5a, b, c). The S_3 foliation consists of four well-developed, non-penetrative conjugate kinks and crenulations, which lie in orthorhombic symmetry about a sub-vertical axis (Figure 4b, c). This geometry is previously unrecognised in kink bands, but is comparable to the geometry of the orthorhombic fault systems reported by Aydin & Reches (1982) and Krantz (1988). The geometry of the kink bands, like the fault systems, implies deformation in response to three-dimensional strain, with dominant ~N-S and subordinate vertical extension (Table 2). Although the direction of maximum shortening remains constant between D_2 and D_3, D_3 represents a rotation of the maximum extension direction from vertical to ~N-S (Table 2). Without obtaining specific age dates from D_3 mineral assemblages the timing of D_3 remains ambiguous with respect to the models of VandenBerg *et al*. (2000). D_3 structures, particularly kink bands, which are common late-stage structures in many orogenic systems (Dewey, 1965), may indicate a continuation of ENE-WSW shortening and therefore the later stages of the Benambran Orogeny. On the other hand, the conjugate D_3 structures may be comparable to the conjugate cross-faults reported by VandenBerg *et al*. (2000), in which case D_3 could represent part of the Tabberabberan Orogeny.

Distinct changes in F_2 plunge and strike are due to the presence of F_3 (Figure 5c). Previous explanations for changes in F_2 plunge included heterogeneous strain during D_2 (Stone, 1937) and transpressional shortening during a later phase of deformation (Forde, 1989). Because of the persistence of F_2 along strike and the anisotropic nature of the sedimentary succession, it is likely that some subtle changes in F_2 plunge are related to heterogeneous strain during D_2. However, the more significant changes in F_2 plunge coincide with a significant change in strike. Simultaneous changes in the strike and plunge of F_2 form well defined zones, which delineate F_3 (Figure 5a, b, c). Transpressional shortening as proposed by Forde (1989) could not have caused these changes in F_2 plunge because the zones defined by a change in plunge and strike (F_3) imply N-S extension not shortening.

It is reported that domal culminations on individual anticlines align obliquely to the strike of F_2 (e.g. Figure 2 in Stone, 1937) and that the most economically significant mineralisation was usually encountered on the north-plunging side of the culminations (Whitelaw, 1914; Stone, 1937; Chace, 1949; Thomas, 1953b). The orientation and geometry of F_3 corresponds to the alignment of domal culminations across the goldfield. This is an important observation for two reasons. Firstly the recognition of F_3 gives a new explanation for the observed outcrop pattern at Bendigo, and secondly, the presence of F_3 may explain why historically the most economically significant mineralisation was encountered on the north plunging side of the culminations. The largest recognised F_3 fold (Figure 5b, c) is situated at the centre of the goldfield and has axial surfaces that dip towards the north. If the historical literature is correct, it is feasible that the D_3 kinks have had an influence on the localisation of gold at Bendigo.

Deformation associated with D_4 implies ~N-S shortening and that a rotation of the principal shortening axis has occurred (Table 2). The S_4 foliation is a non-penetrative, west striking foliation characterised by crenulations and well-developed contractional kink bands (e.g. Figure 6e). D_4 kinks vary in size from a planar fabric (S_4) on a millimetre scale, through to metre scale kinks (F_4; Figure 6f).

A comparable period of ~N-S shortening has been recognised at Bendigo, Ballarat, St. Arnaud and Inglewood by Forde, (1989) and at Stawell by Wilson *et al*., (1992); Miller *et al*., (2001); Miller & Wilson, (2002, 2004). At the Nagambie gold deposit (Gao *et al*., 1995), which is located in the north-eastern part of the Melbourne Zone, auriferous mineralisation is associated with east-west orientated folds and faults. It is suggested by

Gao *et al*. (1995) that these structures are related to a north-south shortening event, thought to have occurred during the Late Devonian. Morand *et al*., (1997) suggest that a weak northwest trending cleavage exists throughout much of the Melbourne Zone and is related to a northeast-southwest compressional event that may represent the latest stages of the Tabberabberan Orogeny (c.f. Gray and Mortimer, 1996). Gray & Willman (1991c) relate two overprinting crenulation cleavages to the strike-slip reactivation of the Heathcote Fault Zone, with initial dextral movement followed by a weaker sinistral movement. It is suggested that the dextral movement is associated with the Tabberabberan Orogeny and that the later sinistral movement might possibly relate to the Middle Carboniferous Kanimblan Orogeny (Gray & Willman, 1991c). VandenBerg *et al*. (2000) recognise that the eastern part of the Bendigo Zone has been affected by a period of north-south shortening late in the Tabberabberan Orogeny. Dextral movement along the Heathcote Fault Zone and other smaller faults, the formation of east- and northeast-trending megakinks (e.g. the Tooborac Megakink) and the existence of a second-generation northwest trending cleavage are related to this north-south shortening event (VandenBerg *et al*., 2000).

It is evident that widespread north-south shortening affected the Melbourne Zone and eastern part of the Bendigo Zone during the later stages of the Tabberabberan Orogeny. The northwest trending foliations recognised by Gray & Willman (1991c), Morand *et al*., (1997) and VandenBerg *et al*. (2000) may be comparable to the S_4 foliation recognised by this study.

Work carried out along the east coast of Victoria and NSW, and across northeast Tasmania has also recognised contractional kink bands, which postdate D_2 and have geometries comparable to the D_4 kinks observed at Bendigo (e.g. Powell *et al*., 1985; Stubley, 1990; Goscombe, *et al*., 1994). Powell *et al*. (1985) hypothesises that kinking involved a continent-wide stress field and that the shortening experienced in the eastern LFB was related to the N-S shortening in central Australia during the Carboniferous Alice Springs Orogeny. If this is the case, then despite their similarities it is likely that the kink bands observed in the Eastern Sub-province post-date those observed at Bendigo.

A second episode of ~N-S shortening, that postdates both D_4 and Jurassic dyke emplacement has been recognised at Bendigo for the first time (Figure 8c, d). Because the extent of the deformation remains unclear and no associated tectonic foliation has

been recognised, this phase of deformation is not interpreted as a period of regional deformation. However, this period of N-S shortening is of great economic significance to the goldfield because the late-stage reactivation of faults has in places, resulted in the truncation of potentially economic mineralisation (Figure 8a, b).

The similarities between this study and Forde (1989) suggest that the S_1-S_4 foliations recognised at Bendigo may also be present at Inglewood, St. Arnaud and Ballarat (Figure 1b), and that the structural development of the Bendigo Goldfield is similar to other Victorian goldfields. The structural setting of the Bendigo Goldfield may also be comparable to other turbidite-hosted gold deposits outside of the WSP. For example, at the Caribou deposit, Nova Scotia, a significant amount of gold is associated with 'late-stage secondary flexures', which have kink band geometry (Ryan & Smith, 1998).

CONCLUSIONS

1. This work, which builds on that of others, documents four overprinting tectonic foliations (S_1-S_4) and proposes a revised four-stage deformation chronology (D_1-D_4) for the Bendigo Goldfield. The third phase of deformation (D_3) was previously unrecognised and may have significant implications for the localisation of gold at Bendigo.
2. The principal shortening direction during D_1, D_2 and D_3 was sub-horizontal and orientated along an ENE-WSW axis. The S_1 and S_2 foliations indicate separate, yet progressive phases of deformation within the one orogeny (Benambran?). Without specific age dating the timing of S_3 remains ambiguous because the foliation could represent the later stages of the Benambran Orogeny or part of the younger Tabberabberan Orogeny. The fourth foliation (S_4) indicates that a significant re-orientation of the principal shortening axis has occurred and as such, D_4 may correspond to the later stages of the Tabberabberan Orogeny.
3. The kink bands have an extensional geometry and are arranged in orthorhombic symmetry about a sub-vertical axis. The D_3 kinks are interpreted as having formed in response to three-dimensional strain, with dominant N-S and subordinate vertical extension.

SECTION B

THE THREE-DIMENSIONAL GEOMETRY AND KINEMATICS OF KINK BANDS WITHIN THE BENDIGO GOLDFIELD, VICTORIA, AUSTRALIA

Abstract

Analysis of the deformation chronology preserved within the host rock at Bendigo, Victoria, Australia has revealed that both extensional and contractional kink bands occur throughout the goldfield. The oldest generation of kink bands, which formed during D_3, consist of four sets of conjugate extensional kink bands, of which two sets have sinistral sense and two sets dextral sense. The four sets have an approximately orthorhombic symmetry about a sub-vertical axis. The sinistral kink bands are typically larger and more numerous than the dextral kink bands, and also exhibit slightly larger α and ψ angles, which implies that the principal shortening direction was not normal to the anisotropy exploited during kinking (ϕ = ~88°). It is suggested that the extensional kink bands formed within a triaxial strain field and that the principal shortening direction was sub-horizontal and orientated ENE.

On a goldfield-scale vector analysis of F_2 axial traces has identified kilometre-scale dextral and sinistral kinks, which exhibit extensional geometry. The orientation and simplified geometric parameters of the kilometre-scale kinks are comparable to the millimetre-scale extensional kink bands observed in thin section. The kilometre-scale kinks are therefore interpreted as having formed within the same strain field as the mm-scale extensional kink bands, with an inferred principal shortening direction of 072°. It is proposed that kilometre-scale kinks are significant to the outcrop pattern observed at Bendigo and the three-dimensional architecture of the goldfield.

Small-scale (mm-scale) contractional kink bands post-date the D_3 extensional kink bands. Both sinistral and dextral contractional kink bands have been observed. However these sets are not conjugate. Contractional kink bands have a strong spatial affiliation with extensional kink bands, which appear to have acted as loci for the nucleation of the younger contractional kinks. The geometric parameters of the contractional kink bands agree with the relationships derived from bulk pure shear experiments performed on anisotropic media. The geometry of sinistral contractional kink bands indicates a principal shortening direction of 010°, whilst the geometry of the dextral contractional kink bands indicates a principal shortening direction of 335°. Geometrical differences between sinistral and dextral contractional kinks suggest that they may have formed in response to two separate periods of deformation (D_4 & D_5?).

Key words: Bendigo Goldfield, orthorhombic kink bands, contractional and extensional kink bands.

INTRODUCTION

Kink bands are common structures in foliated rocks and typically occur late in the structural evolution of an orogenic system (e.g. Anderson, 1968; Dewey, 1965; Fyson, 1968; Ramsay, 1962; Powell *et al*., 1985; Stubley, 1990; Goscombe *et al*., 1994). In addition to the studies of naturally occurring kink bands, experiments involving the deformation of various anisotropic mediums have been undertaken in order to investigate the nucleation and growth of contractional kink bands (e.g. Paterson & Weiss, 1966; Donath, 1968; Weiss, 1968; Cobbold *et al*., 1971; Anderson, 1974; Gay & Weiss, 1974; Weiss, 1980). Although the analysis of experimental data has advanced understanding of kinking mechanisms, comparisons between the geometric properties of naturally occurring and experimentally derived kink bands frequently reveal inconsistencies (e.g. Anderson, 1968; Cudahy, 1986; Stubley, 1990; Kirschner & Teixell, 1996). There are two main discrepancies reported in the literature; the first is between the stress-strain relationships derived experimentally (e.g. Gay & Weiss, 1974) and those inferred from natural kink band systems (e.g. Anderson, 1968; Cudahy, 1986; Stubley, 1990), whilst the second relates to kink band geometry. Several studies of naturally occurring kink bands report geometries that differ significantly from those derived experimentally (e.g. Stubley, 1990; Kirschner & Teixell, 1996). In such cases no single experimental/theoretical model can explain the development of the naturally occurring kink band system.

This contribution investigates the three-dimensional geometry of mm-scale extensional and contractional kink bands observed at Bendigo, Victoria, Australia. The geometric properties of the contractional kink bands are compared to those derived experimentally. Two-dimensional geometric parameters are presented for D_3 kilometre-scale kinks and a comparison is made with the mm-scale D_3 kink bands observed in thin section.

GEOLOGICAL SETTING

Regional geology

The Bendigo Goldfield is situated within the Western Subprovince (WSP; Gray *et al*., 1997) of the Lachlan Fold Belt (LFB; Glen, 1992; Gray & Foster, 1998, 2004; Foster & Gray, 2000; VandenBerg *et al*., 2000; Gray *et al*., 2002), approximately 130 km

northwest of Melbourne, Victoria, Australia (Figure 1a, b, c). The geology of the WSP is dominated by a monotonous succession of deformed and metamorphosed Cambro-Ordovician to Silurian turbidites (Cas & VandenBerg, 1988; Gray & Foster, 2000; VandenBerg *et al*., 2000; Fergusson, 2003). The metasediments are characteristic of medium-P/T (Barrovian type) conditions and predominantly exhibit prehnite-pumpellyite facies metamorphism (Offler *et al*., 1998). The principal style of deformation observed across the WSP has been attributed to a thin-skinned style of crustal shortening, with the formation of a predominantly east-vergent, N-S to NW-SE striking, fold and thrust belt (Gray & Willman, 1991a, b, c; Gray *et al*., 1991; Cox *et al.*, 1991b; Foster & Gray, 2000; Gray & Foster, 2000, 2004). The major thrust faults within the WSP define three structural zones, the Melbourne Zone, Bendigo Zone and Stawell Zone (Figure 1b; Gray, 2003).

Geochronological research (Arne *et al*., 1998; Foster *et al*., 1998; Bierlein *et al*., 2001b, c) demonstrates that metamorphism and deformation was diachronous from west to east across the WSP, beginning in the Late Ordovician-Early Silurian (Stawell and Bendigo Zones) through to the Middle Devonian (Melbourne Zone). Foster *et al*. (1998) Bierlein *et al*. (2001b, c) conclude that the fold and thrust belt of the WSP formed as a result of an eastward-migrating deformation front during the Late Ordovician to Middle Devonian. These findings, which are in general agreement with others (e.g. Collins & Vernon, 1992; Arne *et al*., 1998; Ramsay *et al*., 1998) rule out a synchronous, province-wide mineralising event and instead suggest that gold mineralisation was episodic and associated with both regional metamorphism and the later stages of deformation (Bierlein *et al*., 2002).

Dyke swarms and felsic to intermediate intrusions with S- and I-type affinities were emplaced during two broad intervals. The first, during the Late Silurian to Early Devonian (~415-395 Ma), occurred primarily across the Stawell Zone and south-western, western and north-central parts of the Bendigo Zone, whereas the second affected the entire Melbourne Zone, most of the Bendigo Zone and the eastern part of the Stawell Zone during the Middle to Late Devonian (~385-365 Ma; Richards & Singleton, 1981; Foster *et al*., 1998; Bierlein *et al*., 2001b, c, d). A younger generation of lamprophyre dykes has been dated at 155 Ma (Jurassic) by McDougall & Wellman (1976).

Figure 1. *A. The Lachlan Fold Belt in mainland Australia (LFB). Adapted from Gray* et al. *(1997). B. Subprovinces within the LFB and the location of the Stawell, Bendigo and Melbourne structural zones. Adapted from Gray* et al. *(1997). C. The location of Bendigo within the Bendigo Zone (BZ). Adapted from Gray and Willman (1991a).*

Bendigo geology

The Bendigo Goldfield is located within the Bendigo Zone (BZ; Gray, 2003; Figure 1b, c) where it lies within a 9 km wide NNW trending zone of deformed, Lower to Middle Ordovician turbiditic metasediments bound by the intrazone, west-dipping Whitelaw and Sebastian thrust faults to the east and west respectively (Figure 2). The Ordovician metasediments, which typify the Bendigo region, exhibit rapid and distinct facies changes and belong to a succession of sandstones, siltstones, shales, thin polymict conglomerates and minor cone-in-cone limestones known as the Castlemaine Supergroup (Cas & VandenBerg, 1988; Willman &Wilkinson, 1992).

Figure 2. *Geological map of the Bendigo region, showing biostratigraphic units, intra-zone faults and the Bendigo Goldfield. Adapted from Johansen (2001).*

The structural evolution of the Bendigo Goldfield has been a contentious issue, with as many as three periods of deformation proposed (c.f. Forde, 1991; Schaubs & Wilson, 2002). Section A reinvestigated the structural development of the goldfield and proposed a four-stage deformation chronology (D_1-D_4), based primarily on the recognition of four overprinting tectonic foliations (S_1-S_4).

The first deformation stage (D_1) represents the on set of ~ENE-WSW shortening (Benambran Orogeny, *ca.* 439-435 Ma; VandenBerg *et al*., 2000) and the development of a regionally extensive, N-S to NW-SE trending thrust belt. The morphology, orientation and relative timing of S_1 implies that it formed in response to an early period of layer-parallel shearing, thrust faulting and low grade metamorphism, which occurred prior to the development of F_2 (Forde, 1989, 1991; Wilson *et al*., 1992; Schaubs & Wilson, 2002; Section A).

The second deformation stage (D_2) represents progressive ~ENE-WSW shortening and peak deformation and metamorphism during the Benambran Orogeny. D_2 is characterised by the first generation of mesoscopic folds (F_2) and a well-developed axial planar, differentiated crenulation cleavage (S_2; Forde, 1989, 1991; Cox *et al*, 1991b; Schaubs & Wilson, 2002; Section A), which bestows a strong mechanical anisotropy on the meta-sedimentary succession. A significant episode of quartz veining occurred during the latter part of D_2 with mineralising fluids exploiting the active folds and faults (e.g. Cox *et al*., 1991a; Schaubs & Wilson, 2002).

The third deformation stage (D_3) was first recognised in Section A and represents a period of renewed ENE-WSW shortening and the deformation of F_2 and S_2. The principal structures associated with D_3 are conjugate extensional kink bands and crenulations. The size of D_3 kink bands varies greatly, with small-scale kinks observed on a millimetre scale (S_3) and large-scale kinks at a kilometre scale (F_3). The timing of D_3 is ambiguous and may represent the later stages of the Benambran Orogeny or part of the younger Tabberabberan Orogeny (*ca.* 381-377 Ma; see VandenBerg *et al*., 2000).

The fourth deformation stage (D_4) represents a period of ~N-S shortening (Forde, 1989; Forde & Bell, 1994; Section A), which may correspond to the later stages of the Tabberabberan Orogeny. S_4 is a non-penetrative, west-striking foliation characterised by well-developed contractional kink bands. D_4 kink bands vary in size from a planar fabric (S_4) on a millimetre scale, through to metre scale kinks (F_4).

ANALYTICAL PROCEDURE

In order to investigate the microstructures and microstructural history preserved within the host rocks at Bendigo, approximately 80 orientated pelitic to semi-pelitic samples were collected from exposure both at surface and underground. Suites consisting of fifteen thin sections were cut for 4 samples (C102, G131, G134 & S3109) and included horizontal, N and P sections, and intermediate sections with dips of 20°, 40° and 60° (see Figure 3a, b). The suites of thin sections made it possible to investigate the three dimensional geometry of mm-scale D_3 and D_4 kink bands.

During this investigation only thin sections containing three or more clearly defined kink bands of the same set (e.g. S_{3a}) were utilised. The geometric properties of the small-scale kink bands (Figure 4a, b) were determined by measuring the bearing or pitch of the kink band axial planes and the internal and external foliations for each thin section within a suite (Appendix C, Part 2). The resultant cumulative data was plotted on lower-hemisphere, equal-area stereonets and great circles constructed to define the orientation of the kink band axial planes, internal foliation and external foliation for each set of kink bands ($S_{3a, b, c, d}$ & S_4) within that sample (Figure 5a, b, c). These parameters subsequently allowed the orientation of the fold hinge and the geometric parameters shown in Figure 4a, b to be measured as shown in Figure 5d.

The total error in determining α, β and ψ angles from thin section is estimated to be ± 9°. This value consists of errors (± 8°) incurred during the orientation and preparation of hand specimens and thin sections (Bell *et al*., 1997), and a precision error of ± 1° for measurements made from the thin sections. All two-dimensional directional data presented in this contribution has been analysed in the circular scheme (Mardia, 1972; Fisher, 1993) and vector means calculated where necessary.

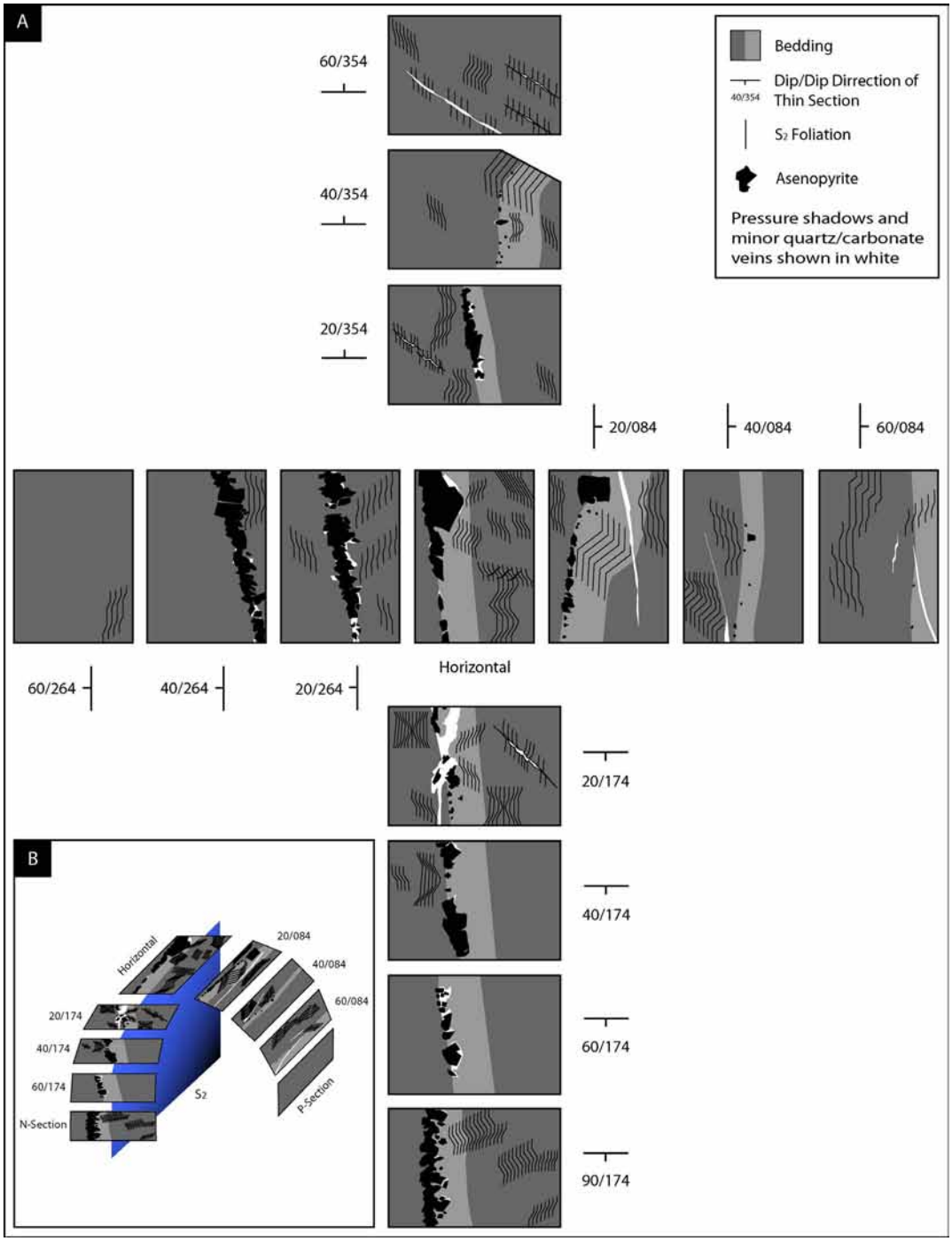

Figure 3. *A. Schematic showing the orientation of 14 thin sections from the suite produced for sample G134. Kink band geometries and relationships have been simplified for clarity. B. Three-dimensional representation of a number of thin sections from the suite produced for sample G134.*

A

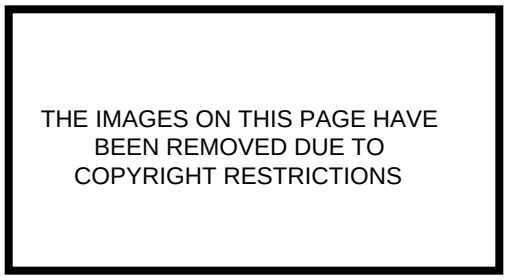

B

Figure 4. *A. Idealised geometry and geometric parameters for conjugate 'contractional' kink bands. B. Idealised geometry and geometric parameters for conjugate 'extensional' kink bands. Adapted from Ramsay & Huber (1987).*

Symbol definitions: The orientation of the kink band axial surface (K_{as}) with respect to the external foliation (K_e) is defined by the angle α. The orientation of the internal foliation (K_i) with respect to the kink band axial surface is defined by β. For contractional kink bands $\alpha + \beta < 180°$, whereas for extensional kink bands $\alpha + \beta > 180°$. The angle through which the internal foliation has been rotated by the kink band is defined by ψ. The orientation of the principal shortening direction (ε_Z) with respect to the external foliation is defined by ϕ.

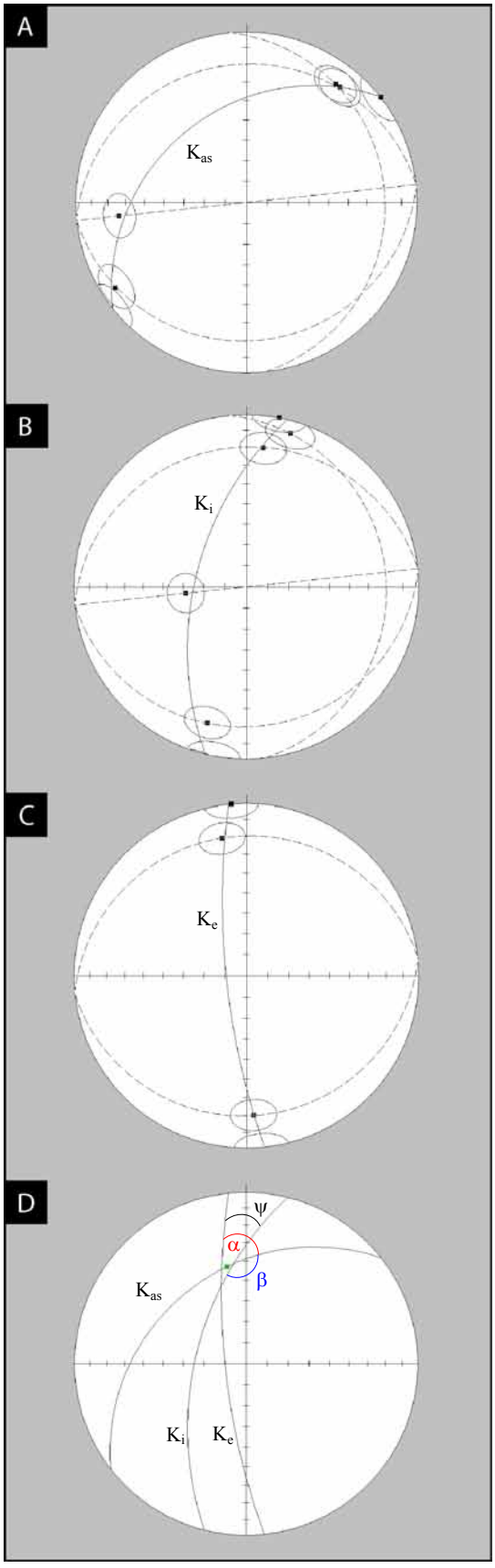

Figure 5. *Determination of kink band geometry (sample G134). A dashed great circle represents the orientation of a thin section, whereas a black square represents the vector mean orientation of a set of kink bands within that section. The circles which encompass a black square defines the ±9° error associated with the vector mean.*

A. The solid great circle represents the vector mean orientation of S_{3b} axial surfaces (K_{as}). B. The solid great circle represents the vector mean orientation of the internal foliation (K_i). C. The solid great circle represents the vector mean orientation of the external foliation (K_e). D. Lower-hemisphere equal-area stereonet showing the orientation of K_i, K_e and K_{as}. From this stereonet the fold hinge and geometric properties (α, β, ψ) can be measured for S_{3b}.

SMALL-SCALE D_3 KINK BANDS

General features

In thin section D_3 kink bands possess monoclinic extensional geometry (*sensu* Ramsay & Huber, 1987; Figure 4b) and record local layer-parallel extension primarily along S_2. Although S_2 is generally the most intense foliation at Bendigo, local-scale variability in the relative intensity and morphology of S_1 and S_2 means that S_1 may be locally important. The foliation exploited during kinking has therefore been termed the 'dominant anisotropy'. Extensional kink bands (Figure 6a, b, c) are characterised by angular to slightly rounded hinges, planar limbs and planar to curviplanar axial surfaces, which bifurcate in a few instances.

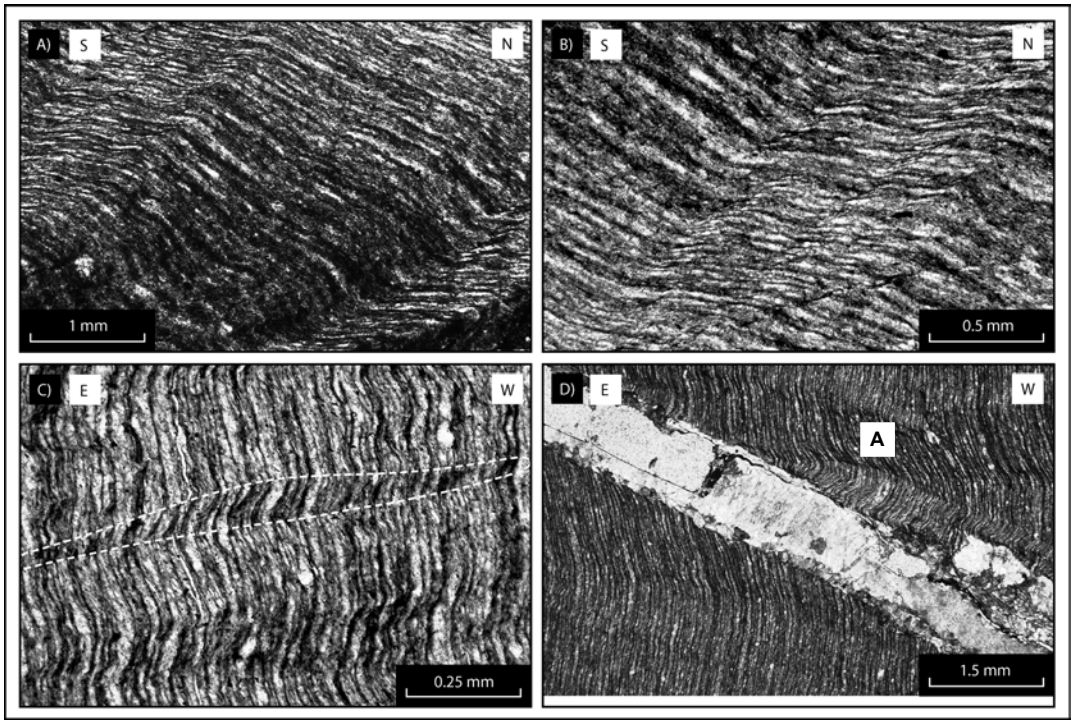

Figure 6. *A. Extensional kink bands that deform S_2/S_1. PPL. Thin-section dips at 20° towards 084°. Sample G134. B. Compound kink (Donath, 1968) that deforms S_2/S_1. PPL. Thin-section dips at 20° towards 084°. Sample G134. C. Lenticular morphology of a small extensional kink band (outlined by white dashed line). Below the lenticular kink band, another kink appears to bifurcate. The foliation deformed by kinking is S_2. PPL. Thin-section dips at 90° towards 354°. Sample G134. D. Deformation of an extensional kink band (labelled 'A') due to the development of flanking structures. PPL. Thin-section dips at 90° towards 354°. Sample G134.*

The internal structure of the kink bands is relatively simple in the majority of cases, with only subtle variations in the parallelism and planarity of the internal foliation. Complex internal structures are uncommon but when observed, result from either the presence of parasitic kinks and crenulations or the occurrence of two or more kink bands in close proximity. In the case of the latter these complex structures may be a form of compound kink (Donath, 1968; Figure 6b). Parasitic kink bands and crenulations are entirely contained within the host kink band. They are orientated parallel to sub-parallel with the host kink band and always exhibit the same sense. Extensional kink bands are best developed in pelitic units and in a few instances exhibit a near "ideal" geometry (Weiss, 1980).

Small-scale extensional kink bands predominantly exhibit a lenticular morphology and terminations defined by a low angle convergence of the axial surfaces (Figure 6c). It is not uncommon for the small-scale kink bands to terminate abruptly against a horizon defined by a marked increase in competency. For example, small-scale kink bands are not observed crossing into or within arenaceous units, suggesting that the more competent units have prevented the propagation and nucleation of small-scale kink bands. Abrupt terminations are also observed where kink bands have intersected quartz veins, carbonate veins or large sulphide grains. Due to the development of flanking structure (Passchier, 2001; Grasemann & Stüwe, 2001) the geometry of small-scale kink bands can become distorted proximal to some veinlets (Figure 6d).

Associated with the extensional kink bands are four distinct types of veinlet:

1. Quartz veinlets with a rectangular or rhombic geometry (Figure 7a). The formation of conjugate extensional kink bands and associated N-S extension has in places resulted in foliation boudinage (e.g. Cobbold *et al*., 1971; Platt & Vissers, 1980). The resultant dilation associated with boudin necks has been exploited by this type of quartz veining.
2. Quartz veinlets that constitute the entire internal portion of a kink band (Figure 7b). These veinlets overprint and preserve the rotated internal foliation, which implies that they formed sometime after the initial development of the kink band. Sharp vein margins define the kink band axial planes and it is suggested that the veinlets formed within permeable kink bands syn-propagation. This type of veinlet is rare indicating that most kink bands either had low permeability or

that there was poor connectivity between kink bands and fluid pathways.

3. En echelon sets of discontinuous lenticular veinlets composed of white mica (Figure 7c). The en echelon veinlets have irregular margins and are consistently inclined at a low angle to the kink axial surfaces. The characteristics and geometry of the veinlets indicates dilation along an axis at a low angle to S_2 and the brittle failure of the layer silicates.

4. Thin planar veinlets composed of white mica orientated perpendicular to the internal foliation and contained solely within a kink band (Figure 7d). These veinlets exhibit irregular margins indicating a, which define the internal foliation. The axis of dilation associated with these veinlets is consistent with the layer parallel extension attributed with the host kink band.

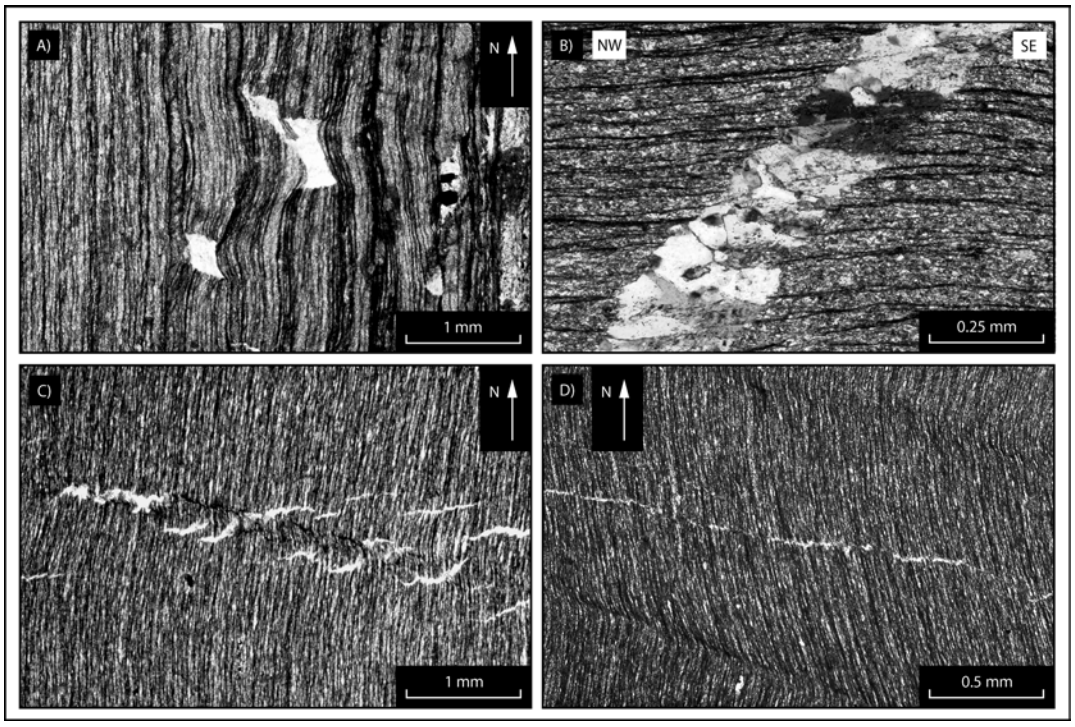

Figure 7. *Four types of veinlet associated with extensional kink bands. A. Foliation boudinage associated with kink band development. PPL. Horizontal thin section. Sample G131. B. Quartz has replaced the internal portion of a kink band and partially preserved the internal foliation. The ψ angle is small due to the obliquity of the thin section to the kink band axial surfaces. XPL. Thin-section dips at 20° towards 245°. Sample G131. C. Millimetre scale en echelon veinlets of white mica. PPL. Horizontal thin section. Sample G134. D. Veinlet comprised of white mica contained within an extensional kink band. The veinlet is orientated perpendicular to the extension direction exhibited by the internal foliation. PPL. Horizontal thin section. Sample G134.*

Geometric features

Conjugate pairs of extensional kink bands are most frequently observed in horizontal and sub-horizontal thin sections. The sinistral and dextral kink bands exhibit 'neutral intersections' where neither kink visibly offsets the other. Although the sinistral and dextral kink bands demonstrate a coeval relationship, the sinistral kink bands are typically larger and more numerous.

For samples C102, G131 and G134 the small-scale extensional kinks observed in thin section consist of four sets of conjugate kink bands ($S_{3a, b, c, d}$), which exhibit an approximate orthorhombic symmetry about a sub-vertical axis (Figure 8a, b, c). The four sets of kink bands consist of two ~WNW-ESE striking sinistral kinks with opposing dip directions ($S_{3a, c}$) and two ~NE-SW striking dextral kinks, also with opposing dip directions ($S_{3b, d}$). For sample S3109 only two sets of conjugate extensional kink bands were recognised (Figure 8d). The two sets of kink bands have the orientation of S_{3a} (sinistral) and S_{3b} (dextral).

Although the strike and dip of the kink band axial planes is tightly constrained within each sample, there is noticeable inter-sample variability (Figure 8). This variability is most likely the result of post D_3 deformation, in particular, transpressional shortening during D_4 (see Section A).

The apparent α angles have been plotted against apparent β angles for every pair of measurements made (Appendix C, Part 2). The four sets of kink bands all demonstrate substantial variability in apparent α, β and ψ angles (Appendix C, Part 2), even between consecutive thin sections (e.g. sections orientated at 20/084 & 40/084).

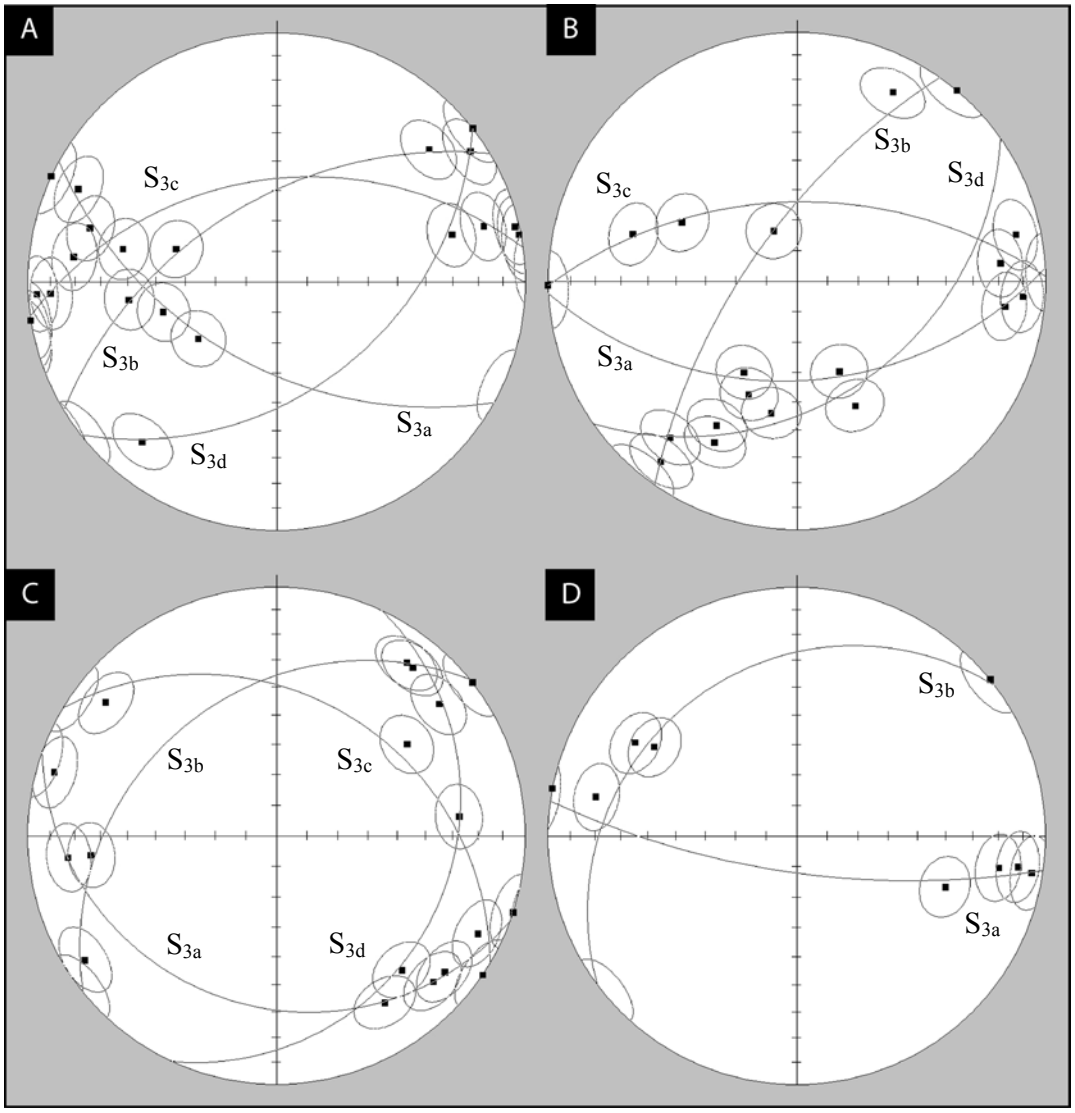

Figure 8. *Lower-hemisphere equal-area stereonets showing the orientation of D_3 extensional kink bands observed within: A. Sample C102. B. Sample G131. C. Sample G134. D. Sample S3109. The black squares are vector means and represent the apparent orientation of a set of kink bands within a thin section (see Figure 5a). The circles which encompass the black squares define the ±9° error associated with each vector mean.*

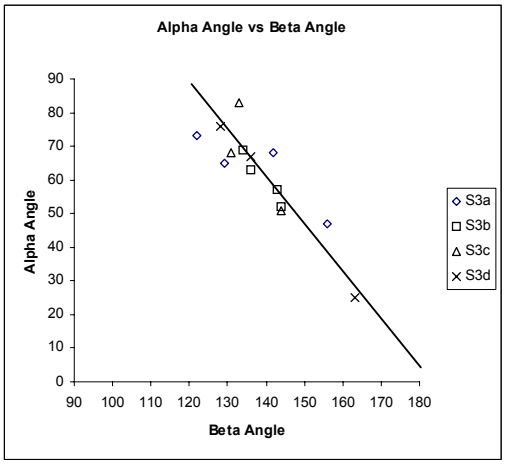

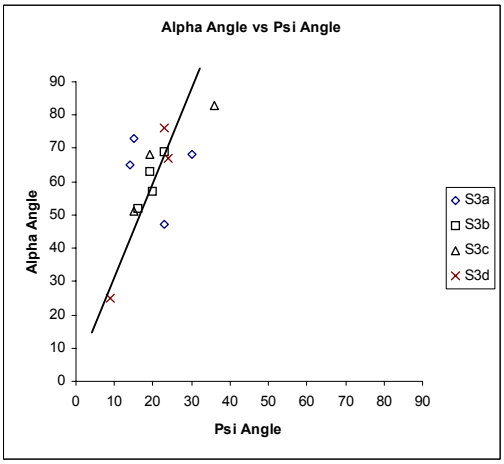

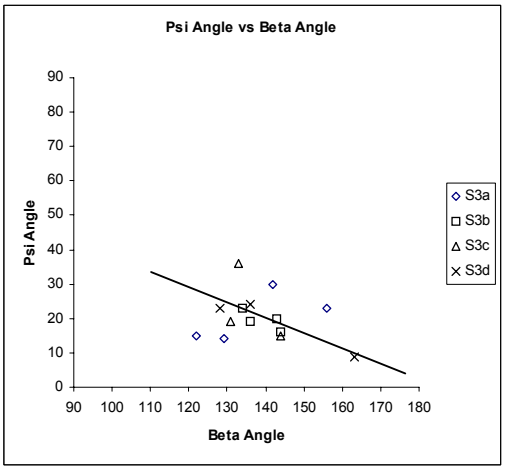

Figure 9. *Plots of geometric parameters of D_3 extensional kink bands. S_{3a} and S_{3c} are sinistral, whereas S_{3b} and S_{3d} are dextral. Linear regression lines shown.*

Discussion pertinent to the three-dimensional geometric features of D_3 kink bands has been simplified by treating the kinks in two categories: sinistral and dextral. The simplification is proposed on the basis that the four sets of kinks display conjugate relations and that the two sets of sinistral kink bands ($S_{3a, c}$) exhibit similar geometric properties, as do the two sets of dextral kink bands ($S_{3b, d}$; Figure 9 & 10). The definition of sinistral and dextral kink bands is base on the sense of rotation when viewed down plunge of the intersection axis between the kink axial surface, the internal foliation and the external foliation (e.g. Figure 10). Lower-hemisphere equal-area stereonets showing kink hinge orientations for each sample are presented in Figure 10, whilst summary statistics for α, β and ψ are presented in Table 1. Subtle geometrical differences between sinistral and dextral kink bands (Table 1 & Figure 11) indicate that the development of sinistral and dextral kink bands was slightly disproportionate.

Table 1. *α, β and ψ angles for sinistral and dextral kink bands within samples C102, G131, G134 and S3109. Angles are in degrees.*

	Sinistral Kink Bands		
	α angle	**β angle**	**ψ angle**
Mean	65	137	22
Minimum	47	122	14
Maximum	83	156	36
Range	36	34	22
Standard Deviation	12	11	9
	Dextral Kink Bands		
	α angle	**β angle**	**ψ angle**
Mean	58	141	19
Minimum	25	128	9
Maximum	76	163	24
Range	51	35	15
Standard Deviation	17	11	5

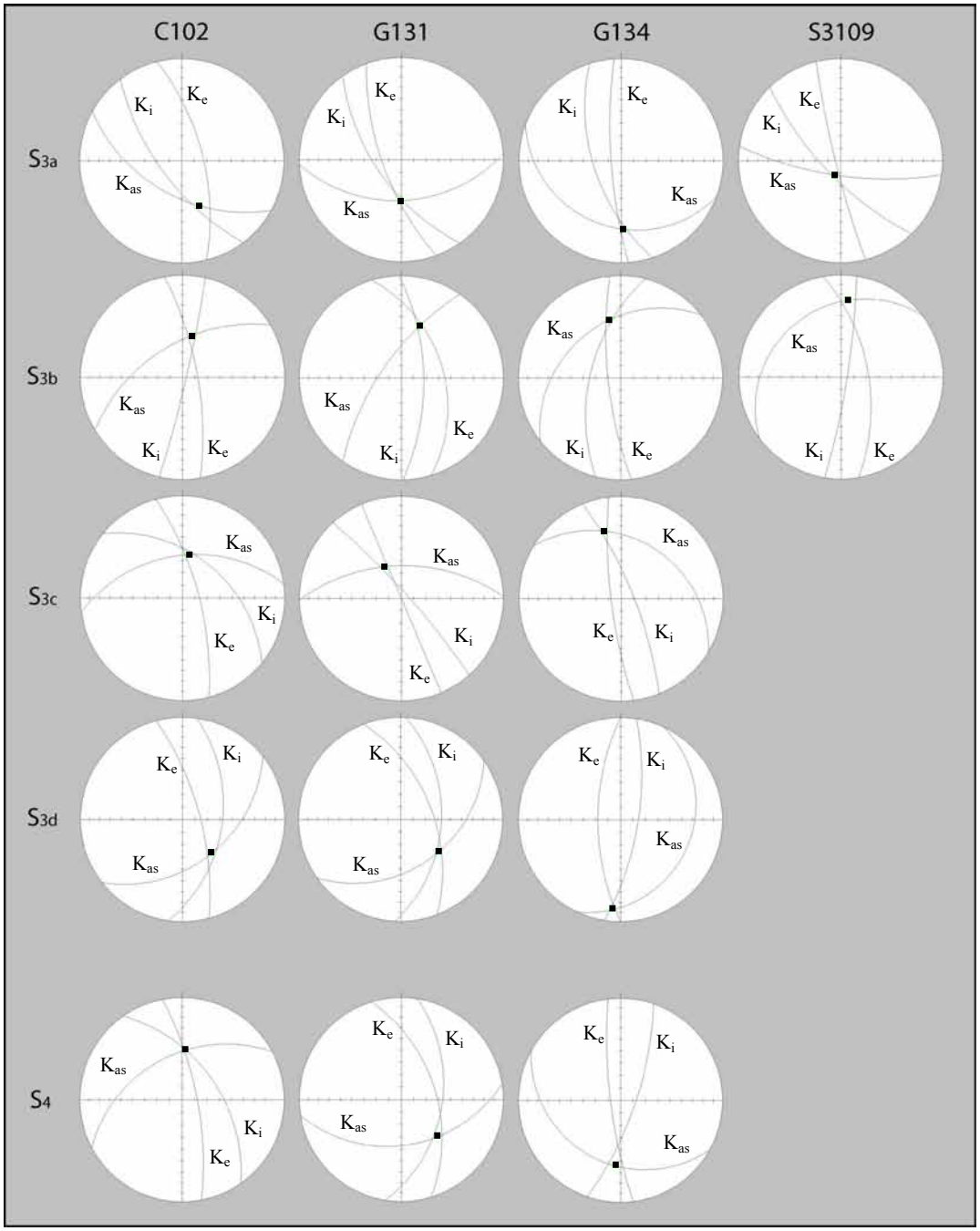

Figure 10. *Summary lower-hemisphere equal-area stereonets for D_3 extensional kink bands (S_3) and D_4 contractional kink bands (S_4). Sample numbers are given. K_{as} represents the axial surface, K_i the internal foliation and K_e the external foliation. The geometric relationship between K_{as}, K_e and K_i is shown in Figures 4a, b & 5d. The squares plotted on K_{as} represent the kink band hinges.*

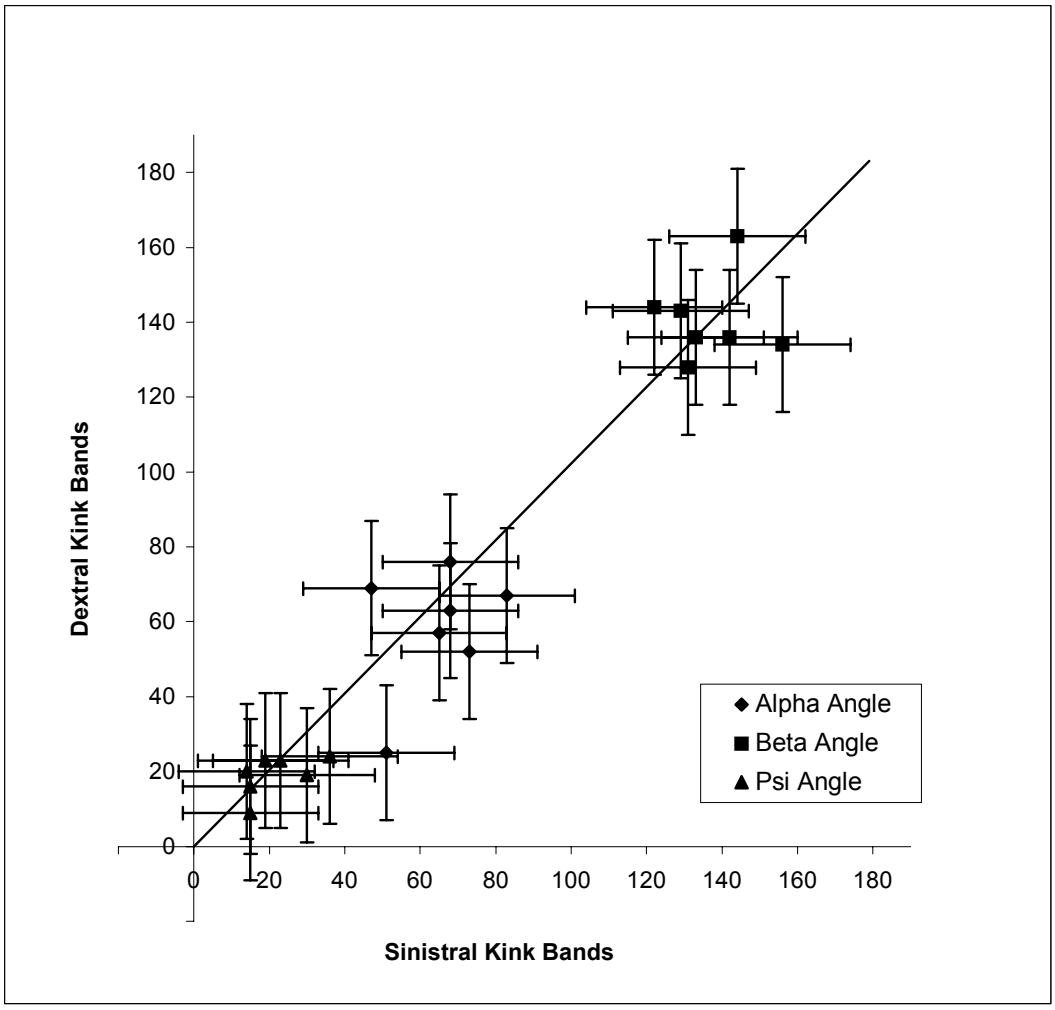

Figure 11. *Plot of geometric parameters with S3a and S3c plotted against S3b and S3d respectively. The geometric relationships of S3a to S3b and S3c to S3d are shown in Figure 8. The data plotted are resultant values as determined for each set of kink bands within each of the four samples. Error bars set at ±9°.*

Principal shortening direction from small-scale kink bands

The D_3 principal shortening direction has been estimated using the 'conjugate bisector' method of Ramsay (1962). It has only been possible to apply the conjugate bisector method to kink bands within samples S3109. This is because the presence of four sets of conjugate kink bands within samples C102, G131 and G134 (Figure 8a, b, c) does not permit the application of the conjugate bisector method.

The geometry of the conjugate kink bands in sample S3109 implies a shortening direction of 076° (Figure 12). The vector mean orientation of the external foliation

within sample S3109 is 68° towards 078°. This implies that ε_z was orientated along a sub-horizontal axis ~2° anticlockwise of normal to the dominant anisotropy. The observation that sinistral kink bands are generally larger, more numerous and characterised by slightly greater α and ψ angles (Figure 11 & Table 1) indicates that the conjugate kink bands are unequally developed relative to the dominant anisotropy. This may explain why the conjugate bisector method would yield an orientation for ε_z that was not normal to the dominant anisotropy but anticlockwise of normal.

The symmetry of the four sets of conjugate kink bands in samples C102, G131 and G134 suggests that the principal strain axes are sub-vertical, NNW-SSE and ENE-WSW. The sense on the kink bands and the orientation of D_3 veinlets observed in thin section implies that ε_z is ENE-WSW, ε_x is NNW-SSE and that ε_y is sub-vertical.

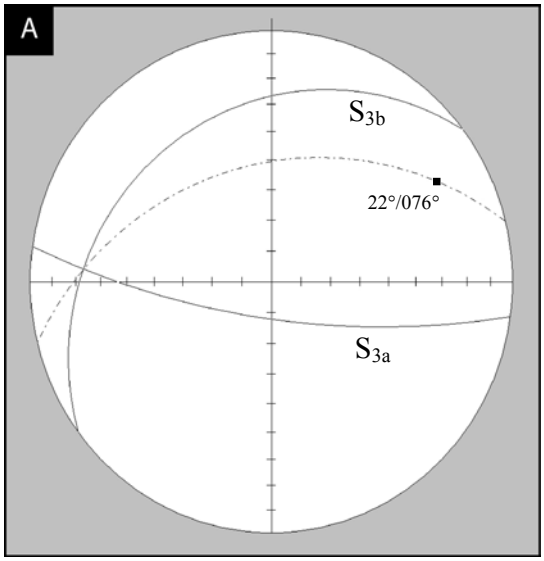

Figure 12. *Lower-hemisphere equal-area stereonets showing the principal shortening direction derived for small-scale extensional kink bands observed within sample S3109. The solid great circles represent the vector mean orientations of the small-scale kink bands. The Dashed great circle represents the orthogonal bisector between the conjugate sinistral and dextral kink bands.*

KILOMETRE-SCALE D_3 KINK BANDS

This study first identified D_3 kilometre-scale extensional kink bands at Bendigo through a reinterpretation of existing 1:10,000 geological maps (Willman and Wilkinson, 1992). In order to accurately define the kilometre-scale kinks within the goldfield, the strikes of the F_2 axial traces were analysed by measuring the orientations of segments between points digitised at intervals of 2 – 65 metres (Appendix B, Parts 1 & 2). Centre points

between the digitised nodes of F_2 axial traces were generated and the orientation of the line that joined the adjacent nodes was assigned to the respective centre point. The analysis of the F_2 axial traces utilises in excess of 10,000 centre points constructed from 10 adjacent F_2 anticlines (Appendix B, Part 1 & 2). Despite the high density of data points, three potential problems have been recognised. The first relates directly to the original mapping, where the inevitable extrapolation of axial traces across unmapable areas may have smoothed any change in strike. The second potential problem is that further smoothing may have occurred when the axial traces were digitised from the 1:10,000 geological maps. The third potential problem is that there is no definitive way of distinguishing kink-related deformation from deformation caused by, for example, oblique faults.

In an attempt to address the latter, dextral and sinistral rotations (ψ) in the strike of F_2 equal to or greater than 9° from the vector mean (345°) have been plotted (Figure 13a, b). The value of 9° was determined from the analysis of extensional kink bands observed in horizontal thin sections (Appendix B, Part 3). A top cut has also been applied to the ψ data to remove extreme values thought unrealistic of kink band development (Appendix B, Part 3). The impact of any smoothing is considered to be minimal because firstly, breaks in the continuity of outcrop are minimal, particularly along strike of F_2 anticlines and secondly, the orientation of F_2 axial traces on current geological maps resembles closely the axial traces depicted on early maps made prior to significant urbanisation (e.g. Herman 1923; Figure 2 in Stone, 1937; Figure 2 in Thomas, 1953b). Also, the apparent width of the kilometre-scale kinks is far greater than any natural/artificial cover.

General Features

Axial traces have been constructed for the kinked domains (Figure 13a, b) identified through this method (Figure 14). Four kilometre-scale kinks were defined (Figure 13a, b & 14), two with dextral sense and two with sinistral sense. The individual kink bands possess monoclinic extensional geometry and appear to have complex internal structures. The largest kink (marked S2 in Figure 13b) has the appearance of a compound structure (Donath, 1968).

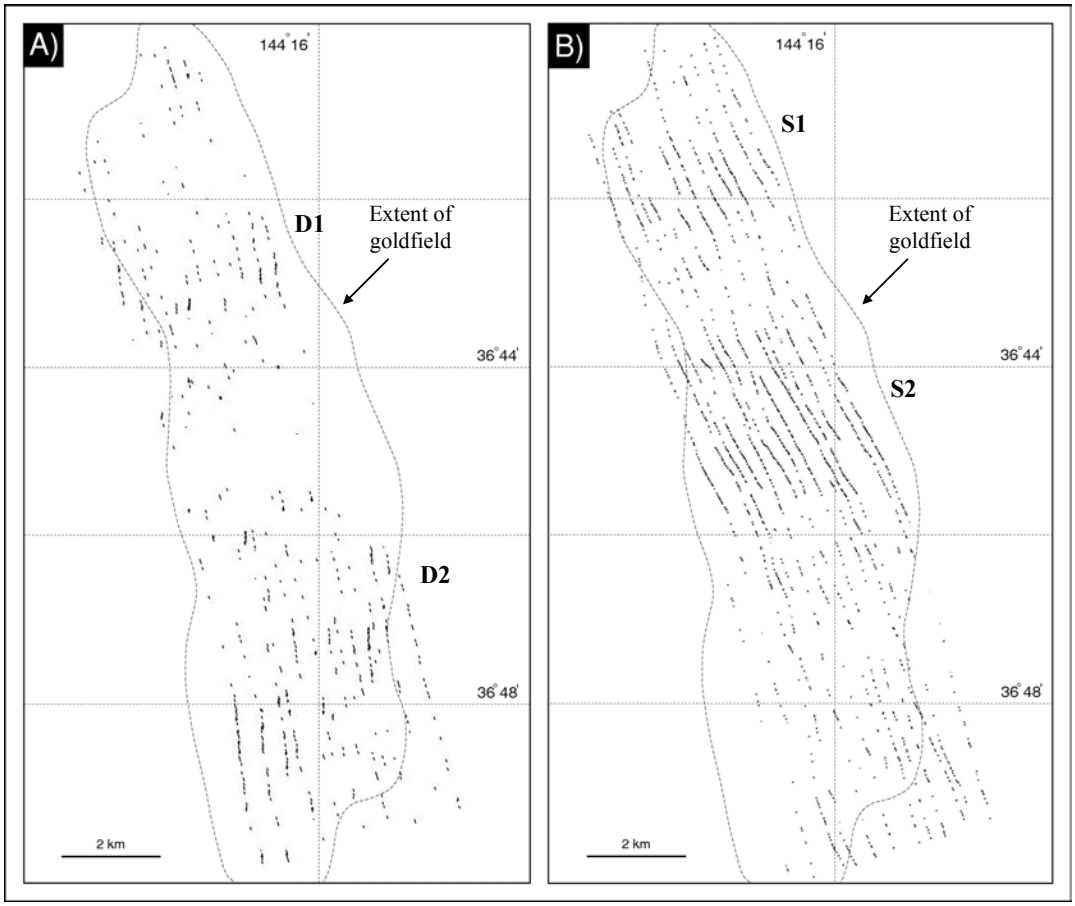

Figure 13. *A. Plot of centre points defined by a dextral rotation in the strike of F_2 equal to or greater than 9° relative to a vector mean of 345°. Modified from Section A. B. Plot of centre points (see text above) defined by a sinistral rotation in the strike of F_2 equal to or greater than 9° relative to a vector mean of 345°. Modified from Section A. Four rotated domains (kinks) are clearly evident; two have a dextral sense (D1 & D2) and the other two a sinistral sense (S1 & S2). The areas between the four kinks are characterised by numerous, less persistent rotated domains, which may indicate a 'mesh' of smaller kink bands.*

In the exposed topographic plane rotations in the strike of F_2 associated with kinking appear quite subtle (Figure 14), which may indicate one or a combination of the following:

1. The intersection of F_3 axial surfaces with the topographic surface is oblique;
2. The original geological mapping and/or subsequent digitisation of the F_2 axial traces has incurred a significant amount of smoothing;
3. The kilometre-scale kink bands exhibit relatively small ψ angles; and

4. The kilometre-scale kink bands exhibit rounded hinges (c.f. Figure 1a, b in Gay and Weiss, 1974).

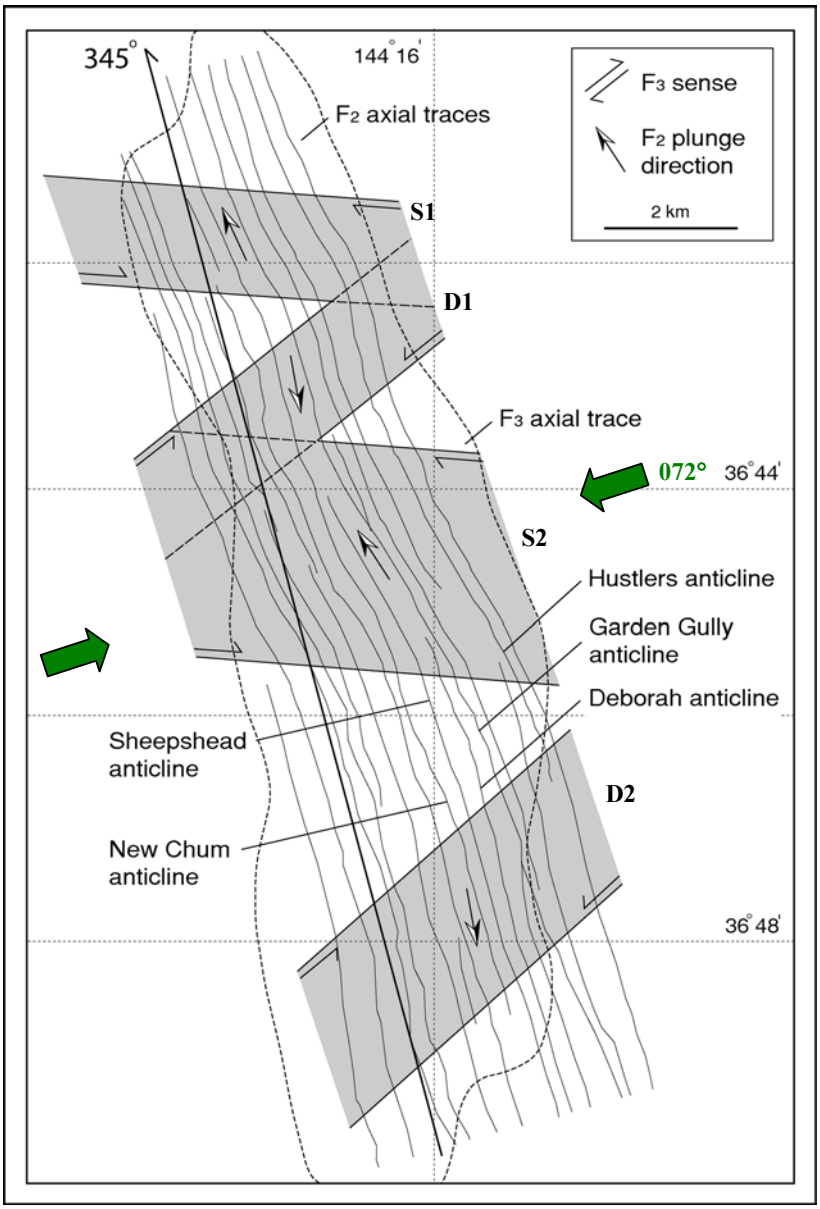

Figure 14. *Kink bands delineated from a reinterpretation of the Bendigo Goldfield 1:10,000 geological maps and vector analysis of the F_2 axial traces. Modified from Section A. Large-scale uniform rotations (F_3) in the strike of F_2 are highlighted in grey (S1, S2, D1 & D2) and represent the rotated domains shown in Figure 13a, b. The general plunge direction of F_2 within F_3 is shown and was determined from the 1:10,000 geological maps for the Bendigo Goldfield. The approximate extent of the goldfield is represented by the thick dashed line, which is also shown in Figure 2. The solid black line represents the vector mean for the F_2 axial traces (345°) as determined from vector analysis. The solid green arrows represent the principal shortening direction (072°) estimated using the conjugate bisector method of Ramsay (1962).*

Sinistral and dextral rotations in the strike of the F_2 axial traces on a smaller scale than those associated with the four major kinks (Figure 14) can be observed across the entire goldfield (Figure 13a, b). These rotations of the F_2 axial traces form more discrete zones, which are considerably more abundant in the southern portion of the goldfield (Figure 13a, b). It is suggested that the existence of these less persistent zones may relate to the following:

1. A network of smaller (<1 km true width) kilometre-scale kink bands; and
2. Other significant structures such as oblique faults (e.g. Willman & Wilkinson, 1992)

The geometric properties of kilometre-scale sinistral and dextral kink bands are summarised in Tables 2 & 3. As well as the potential problems mentioned previously, the geometric data for kilometre-scale kink bands presented in Table 2 are also subject to the assumption that the kink band axial traces remain parallel and planar over the area investigated (Figure 13a, b). The mean α and β angles determined for the sinistral and dextral indicate that they exhibit extensional geometry ($\alpha + \beta = \geq 180°$; s*ensu* Ramsay & Huber, 1987; Figure 4b). The geometric parameters of the kilometre-scale kinks and small-scale kink bands observed in horizontal thin sections show comparable geometries (Table 2). Summary statistics for values of ψ are presented in Table 3. For kilometre-scale kinks ψ angles have been determined using vector analysis and are therefore relative to the vector mean strike of F_2. Consequently, it was to be expected that the mean values of ψ for sinistral and dextral kinks would be similar (Table 2). A comparison of ψ values with those determined for extensional kink bands present in horizontal thin sections reveals strong similarities, the only notable difference is between the maximum values of ψ for dextral kinks (Table 3). In thin section it was observed that the sinistral kink bands were more dominant, which is also apparent on a goldfield scale (compare Figures 13a & 13b). On the basis that the kilometre-scale kink bands have comparable geometries to the small-scale kink bands observed in thin sections (Table 2), it is proposed that the three-dimensional geometries are also similar (e.g. Figure 8 & 10).

Table 2. *Comparison between kilometre-scale kinks, extensional kink bands observed in horizontal thin sections and the resultant three-dimensional geometry of small-scale extensional kink bands. Values quoted for geometric parameters are mean values and in degrees. Dex – Dextral, Sin - Sinistral.*

	Axial Surfaces		External Foliation		Internal Foliation		α		β		ψ	
	Sin	**Dex**	**Sin**	**Dex**	**Sin**	**Dex**	**Sin**	**Dex**	**Sin**	**Dex**	**Sin**	**Dex**
Kilometre-scale Kinks	095	232	345†	345†	328	001	70	67	126	129	17	16
Small-Scale Kinks*	102	229	348	352	325	009	66	58	137	139	23	17
Small-Scale Kinks**	*See Figure 10*						65	58	137	141	22	19

† Vector mean orientation of F_2 axial traces as determined from vector analysis

* Mean geometric parameters of small-scale kink bands observed in horizontal thin sections

** Resultant three-dimensional geometric parameters for small-scale extensional kink bands

Table 3. *Comparison of ψ values for kilometre-scale kinks and extensional kink bands observed in horizontal thin section. Values of ψ are in degrees.*

	Map Scale Kink Bands		Small-Scale Kink Bands (Horizontal Thin Sections)	
	Sinistral	**Dextral**	**Sinistral**	**Dextral**
Mean	17	16	23	17
Minimum	9‡	9‡	6	11
Maximum	48†	43†	41	27
Range	39	34	35	16
Standard Deviation	7	6	9	3
Count	2787	850	180	120

‡ Minimum ψ value determined from horizontal thin sections. Appendix B, Part 3.

† Top-cuts have been applied to remove extreme values of ψ. Appendix B, Part 3.

Principal shortening direction from kilometre-scale kink bands

The approximated geometric parameters of the kilometre-scale kink bands are comparable to the small-scale extensional kink bands observed in horizontal thin sections (Table 2). The slight difference between the mean α angles for sinistral and dextral kink bands implies that the shortening direction was not normal to the anisotropy, but a little anticlockwise of normal (c.f. Gay & Weiss, 1974). The orthogonal bisector (Ramsay, 1962) of the conjugate sinistral and dextral kilometre-scale kink bands (Figure 14) implies an approximate shortening direction of 072°.

Although the kilometre-scale kink bands were investigated in two-dimensions their geometric properties and derived shortening direction are comparable to the small-scale kink bands. On this basis the kilometre-scale kinks are interpreted as having formed within the same strain field as the small-scale kink bands.

SMALL-SCALE D_4 KINK BANDS

General features

In thin section D_4 kink bands exhibit monoclinic contractional geometry (*sensu* Ramsay and Huber, 1987; Figure 4a) and record local layer-parallel shortening. Generally the anisotropy exploited during kinking is the well-developed axial planar foliation S_2, however, local-scale variability in the relative intensity and morphology of S_1 and S_2 means that S_1 may be locally important. The foliation exploited during kinking has therefore been termed the 'dominant anisotropy'. Small-scale contractional kink bands are best developed in pelitic to semi-pelitic units and typically display angular to slightly rounded hinges, planar limbs and planar to curviplanar axial surfaces (Figure 15). Unlike D_3 extensional kink bands there are no new mineral phases associated with the development of D_4 contractional kink bands.

Despite the small size of these kinks their internal structure can be complex in the following aspects:

1. Remnants of small-scale D_3 kink bands have been overprinted by and preserved within larger D_4 kinks (Figure 15b). The D_3 kink bands have an opposite sense of asymmetry to the overprinting D_4 kinks.

2. Minor kinks and crenulations, which are entirely contained within the host kink band (Figure15b, d). The minor kinks and crenulations predominantly exhibit the same sense as the host kink. The minor kink bands are orientated sub-parallel with the host kink band and typically at a lower angle to the unrotated external foliation. These minor kinks may be juvenile kinks that nucleated some time after the host kink band. The sub-parallel relationship between a host and juvenile kink may signify that the central portion of the host kink band rotated during growth (see Figure 6 in Weiss, 1980), prior to the nucleation of the juvenile kink. It is important to note that the direction of longitudinal propagation is the same for both the host and minor kink bands.
3. The internal foliation is 'severely wrinkled' (c.f. Paterson & Weiss, 1966; Figure 15b, d).

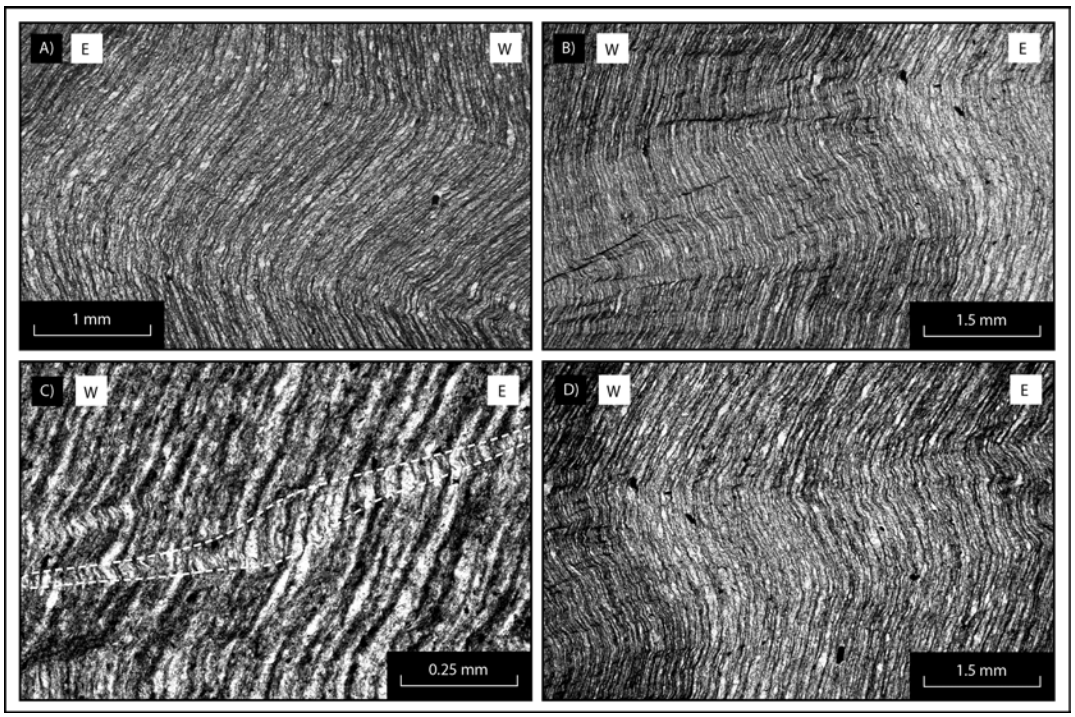

Figure 15. *A. Well-developed contractional kink band that deforms S_2. PPL. Thin-section dips at 90° towards 354°. Sample G134. B. Contraction kink band that deforms S_2 (sub-vertical) and sub-horizontal D_3 extensional kink bands. The kink band contains parasitic kinks and crenulations and remnants of D_3 kink bands. Note the proximity and similar orientation of extensional and contractional kink bands. PPL. Thin-section dips at 90° towards 174°. Sample G134. C. Small contractional kink band, which deforms S_2 and has a sigmoidal geometry. PPL. Thin-section dips at 90° towards 174°. Sample G134. D. Well-developed contractional kink band that deforms S_2. The internal foliation is wrinkled and also deformed by minor kinks and crenulations. PPL. Thin-section dips at 90° towards 174°. Sample G134.*

Small-scale contractional kink bands mostly exhibit a lenticular to subtle sigmoidal morphology and terminations defined by a low angle convergence of the axial surfaces (Figure 15c). Abrupt terminations are observed where small-scale contractional kink bands intersect a horizon defined by a marked increase in competency. For example, abrupt terminations are observed where the longitudinal propagation of a kink band has intersected a quartz vein, carbonate vein or large sulphide grain (Figure 16a, b, c). Due to the formation of flanking structures (Passchier, 2001; Grasemann & Stüwe, 2001) it is not uncommon for the geometry of kink bands to become distorted proximal to some veinlets (Figure 16a, b).

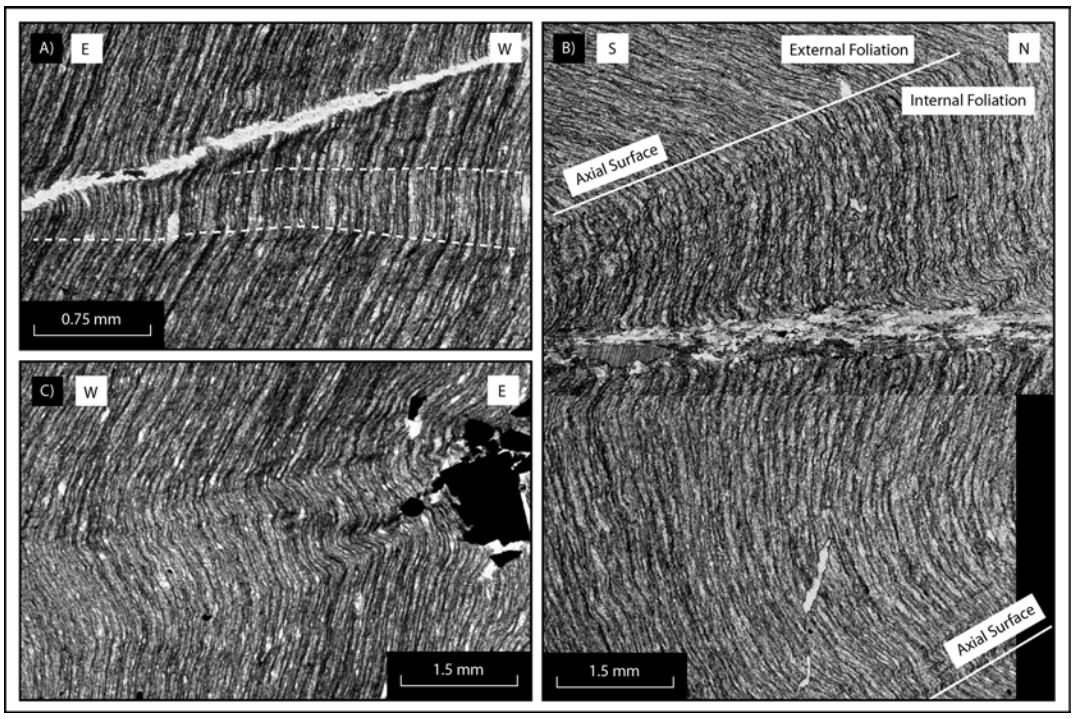

Figure 16. *A. Photomicrograph showing a contractional kink band that distorts where it terminates against the carbonate vein. Axial planes marked by dashed white line. PPL. Thin-section dips at 90° towards 174°. Sample G134. B. Photomicrograph showing the intersection of a mm-scale contractional kink band with a carbonate vein. The formation of flanking structures distorts the internal foliation. Smaller kinks contained within the larger kink terminate against the carbonate vein. PPL. Thin-section dips at 20° towards 084°. Sample G134. C. Contractional kink band with converging axial surfaces that appears to terminate against grains of arsenopyrite. PPL. Thin-section dips at 90° towards 354°. Sample G134.*

As well as terminating against sulphide grains, numerous contractional kink bands can be observed propagating from their margins. This is particularly the case within pelitic

units where sulphide grains form continuous bands parallel to S_1 or S_2. Small-scale contractional kink bands also have a strong spatial affiliation with D_3 kink bands and either overprint the D_3 kinks or occur in close proximity to them (e.g. Figure 15b).

Geometric features

Sinistral and dextral contractional kink bands were observed in three out of the four samples analysed in detail. Sinistral kinks observed in thin sections from sample C102 have a vector mean strike of 062° and a dip of 54° (Figure 17a). The vector mean orientations for dextral kink bands observed in samples G131 and G134 showed some variability, with strikes of 261° and 299° and dips of 38° and 53° respectively (Figure 17b, c).

The dextral contractional kink band axial surfaces have a similar orientation within each sample. However an amount of inter-sample variability is evident (Figure 10 & 17a, b, c). The variation between sample G131 and G134 reflects the important role that extensional kink bands played in the nucleation of the younger contractional kinks. This relationship is further emphasised when the orientation of S_{3a} for samples G131 and G134 (Figure 10) is compared with the orientation of dextral contractional kink bands from the respective samples (Figure 10). Likewise, sample C102 displays the same relationship between S_{3b} and sinistral contractional kink bands (Figure 10).

The apparent α angles have been plotted against apparent β angles for every set of measurements made (Appendix C, Part 2). As with the extensional kink bands, the contractional kink bands demonstrate significant variability in apparent α, β and ψ angles, even between consecutive thin sections (e.g. sections cut at 20/084 & 40/084). Lower-hemisphere equal-area stereonets showing fold hinge orientations and resultant α, β and ψ angles for each sample are presented in Figure 10 and Table 4 respectively.

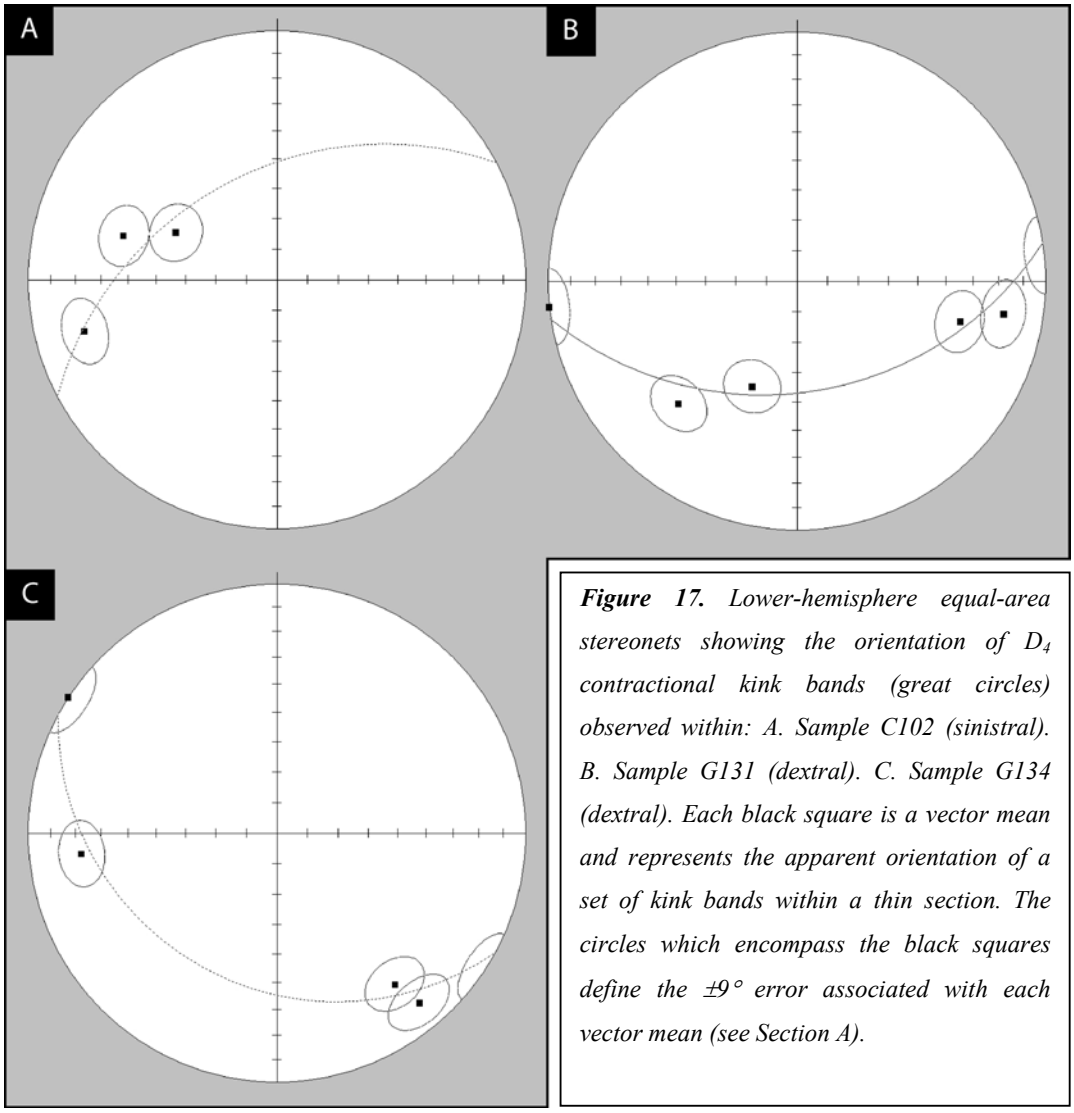

Figure 17. *Lower-hemisphere equal-area stereonets showing the orientation of D_4 contractional kink bands (great circles) observed within: A. Sample C102 (sinistral). B. Sample G131 (dextral). C. Sample G134 (dextral). Each black square is a vector mean and represents the apparent orientation of a set of kink bands within a thin section. The circles which encompass the black squares define the ±9° error associated with each vector mean (see Section A).*

Table 4*. True α, β and ψ angles for sinistral and dextral contractional kink bands determined from sample C102, G131 and G134 (see Figure 10). Angles are in degrees.*

	Sample No.		
	C102 (Sinistral)	**G131 (Dextral)**	**G134 (Dextral)**
α	73	81	54
β	83	72	80
ψ	24	27	26

D_4 principal shortening direction

The D_4 principal shortening direction has been estimated using the experimental data of Gay and Weiss (1974). The coaxial experiments performed by Gay and Weiss (1974) on card decks and slate led to the derivation of relationships between ϕ and α, ϕ and β and ϕ and ψ. The true α, β and ψ values determined in this study for sinistral kink bands in sample C102 (Table 4) have been compared with the experimental data of Gay and Weiss (1974) (Figure 18). For dextral kink bands within samples G131 and G134 mean values have been calculated from the true α, β and ψ angles presented in Table 4. These mean values have also been compared with the experimental data (Figure 18).

For a single set of contractional kink bands ε_z lies within the acute angle between the external foliation and the axial plane (Gay & Weiss, 1974). Mean values for ϕ have been calculated (Table 5) and the orientation of ε_z determined accordingly (Table 6).

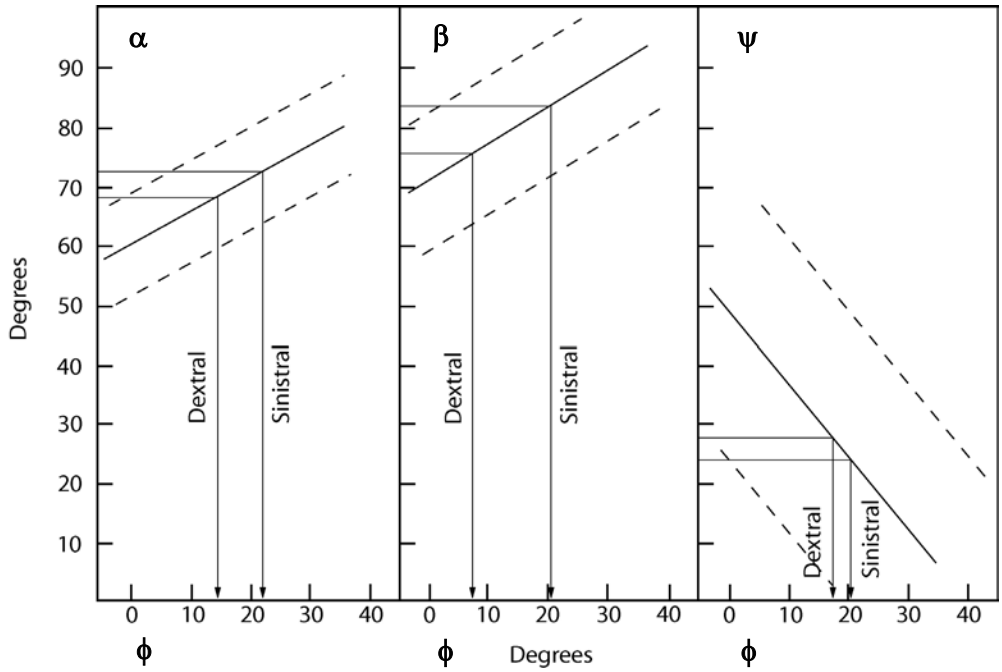

Figure 18. *Plot relating ϕ to α, β and ψ. Solid lines represent best-fit lines through experimental data as defined by Gay and Weiss (1974). Dashed lines are 95% confidence limits. Arrowed lines represent estimates of ϕ from α, β and ψ values. The data plotted is presented in Table 4, arithmetic means were calculated for the dextral kink band data.*

Table 5. *ϕ values derived using the experimental data of Gay and Weiss (1974). Values of ϕ are quoted in degrees.*

Geometric parameters	ϕ values for small-scale D_4 kink bands	
	Sinistral	**Dextral**
α	22	14
β	20.5	7
ψ	20	17
Average ϕ	21	13

Table 6*. Derivation of the D_4 principal shortening direction (ε_z). Values presented are in degrees.*

	Small-scale D_4 kink bands	
	Sinistral	**Dextral**
Average ϕ	21	13
Strike of K_e	349	348†
Bearing of ε_z	010	335

K_e External foliation

† Mean strike of K_e for samples G131 and G134.

DISCUSSION

Small-scale extensional kink bands

Despite a significant amount of research in to the nucleation, growth and geometric properties of experimentally derived and naturally occurring contractional kink bands, very little is known about extensional kink bands. Cobbold *et al*. (1971) deformed a stack of lubricated plasticine layers with compression-applied normal to the layering. The deformation of the plasticine model, which culminated in the development of conjugate extensional kink bands, was reported as being "remarkably similar to the

development of reverse (contractional) kink bands". In this study it is also apparent that extensional kink bands display a number of similarities to contractional kink bands, particularly regarding kinking mechanisms and the relationships between principal shortening directions and kink band geometries.

The geometric properties of the extensional kink bands can be thought of in terms of existing models for the formation and growth of contractional kink bands. The majority of extensional kink bands observed at Bendigo display relatively simple geometries, with only subtle variations in the parallelism and planarity of the internal foliation. This suggests that the extensional kink bands are more likely to have resulted from a kinking mechanism similar to that of the constant-segment-length model (Anderson, 1964; Dewey, 1965; Donath, 1968) than the hinge-migration model (Paterson & Weiss, 1966; Gay & Weiss, 1974; Weiss, 1980). The presence of compound kinks (Donath, 1968; Figure 6b) may also be explained through the constant-segment-length model.

The small-scale (mm-scale) extensional kink bands consist of four sets of conjugate kink bands arranged in orthorhombic symmetry (Figure 8a, b, c). This geometry could not be resolved using horizontal, N- and P-sections and required additional intermediate thin sections to be produced (Figure 3a, b). A similar geometry has been proposed by Kirschner & Teixell (1996) for contractional kink bands located within the Somport formation, central Pyrenees. However, the contractional kinks are highly curved and form an anastomosing network of kink bands, which appears to be incompatible with the geometry of the extensional kink bands presented in this contribution (Figure 8a, b, c) and the models developed for orthorhombic fault systems (e.g. Krantz, 1988). The geometry of the small-scale extensional kink bands observed at Bendigo, which is comparable to the geometry of the fault systems reported by Aydin & Reches (1982) and Krantz (1988), was previously unrecognised in any type of kink band. The geometry of the kink bands, like the fault systems, implies deformation in response to tri-axial strain.

Conjugate kink bands have been considered by numerous authors to be geometrically and kinematically similar to conjugate fault systems (e.g. Kirschner & Teixell, 1996). In light of the geometrical similarities and in an attempt to determine the orientation of the principal strain axes, the 'odd axis' model of Krantz (1988) was applied to kink bands observed in sample G134 (Figure 8c). In applying the odd axis model it was assumed that a kink band was geometrically analogous to a fault, with the slip vector orthogonal

to the kink band hinge (Figure 10). It was found that the principal strain axes could not be resolved using the odd axis model despite the orthorhombic symmetry of the kink bands. It is suggested that the assumption of orthogonal slip vectors may be flawed and/or that a kink band may not be geometrically analogous to a fault in some other way(s). This inevitably raises questions regarding kinking mechanisms that need to be investigated. As a result the principal shortening direction could only be approximated using the 'conjugate bisector' method of Ramsay (1962) (Figure 12).

Principal shortening directions derived using the conjugate bisector method (Figure 12) indicate that ε_z was sub-horizontal and directed along an ENE axis. It has also been shown that ε_z was not normal to the dominant anisotropy during kinking. Instead ε_z was orientated along a sub-horizontal axis ~2° anticlockwise of normal. Gay and Weiss (1974) demonstrate that the angle between the external foliation and the direction of maximum shortening (ϕ) has a direct influence on the number of sets, orientation and geometry of resulting contractional kink bands. It may be possible to consider this relationship in terms of extensional kink bands, where the presence of well-developed conjugate kink bands would imply that ε_z was within 5° of normal, relative to the dominant anisotropy (ϕ = 85-90°; c.f. Figure 4a & 4b).

Kilometre-scale extensional kink bands

On a goldfield-scale (Figure 2) vector analysis of F_2 axial traces has identified kilometre-scale dextral and sinistral kinks, which exhibit extensional geometry. Although vector analysis successfully confirms the existence and location of kilometre-scale kinks at Bendigo, the data are restrictive and only allows the kinks to be investigated in two-dimensions and in a plane that is most likely not orthogonal to the kink band axial surfaces.

The orientation and geometric parameters of the kilometre-scale kinks are comparable to the small-scale extensional kink bands observed in horizontal thin section (Table 2 & 3). Therefore the kilometre-scale kinks are interpreted as having formed within the same strain field as the small-scale extensional kink bands, with an inferred principal shortening direction of 072° (Figure 14). It is proposed that kilometre-scale kinks contribute significantly to the outcrop pattern observed at Bendigo and the three-dimensional architecture of the goldfield.

Small-scale contractional kink bands

Kink bands with contractional geometry have been the focus of numerous studies concerned with the nucleation, growth and geometric properties of experimentally derived kink bands (e.g. Paterson & Weiss, 1966; Donath, 1968; Anderson, 1974; Cobbold *et al*., 1971; Gay & Weiss, 1974; Weiss, 1980) and naturally occurring kink bands (e.g. Anderson, 1964, 1968; Fyson, 1968; Powell *et al*., 1985; Stubley, 1990; Goscombe *et al*., 1994; Kirschner & Teixell, 1996). The geometric properties of the contractional kink bands observed at Bendigo can be thought of in terms of existing models for the formation and growth of kink bands (c.f. Stubley, 1990). The majority of contractional kink bands are characterised by subtle sigmoidal geometry, 'severe wrinkling' (Weiss, 1968) of the internal foliation and the presence of small kinks and crenulations within larger kink bands of the same sense (Figure 15b, d). Similar characteristics are reported in Paterson & Weiss (1966), Gay & Weiss (1974) and Weiss (1968, 1980), which suggests that the contractional kink bands are more likely to have resulted from a kinking mechanism similar to that of the hinge-migration model and not the constant-segment-length model (Anderson, 1964; Dewey, 1965; Donath, 1968).

A striking aspect of the sinistral and dextral contractional kink bands is their strong spatial affiliation with extensional kink bands. Figure 10 shows that the orientation of the dextral contractional kink bands for samples G131 and G134 is comparable to the orientation of S_{3a} from the respective sample. Likewise, sample C102 displays a similar relationship between sinistral contractional kink bands and S_{3b}. This appears to indicate that the older extensional kink bands acted as loci for the nucleation of the contractional kinks. Although the concept of kink bands nucleating and developing along pre-existing structures is not new (e.g. Powell *et al*., 1985; Cudahy, 1986), the nucleation and growth of contractional kink bands along extensional kink bands has not previously been reported. This relationship may explain why there is a notable degree of inter-sample variability in the orientation of the contractional kink bands, particularly given that the kink bands formed late in the structural evolution of the goldfield (see Section A).

Comparisons made between principal shortening directions inferred from naturally occurring kink bands and experimentally derived relationships frequently reveal inconsistencies (e.g. Dewey, 1965; Anderson, 1968; Stubley, 1990; Goscombe *et al*.,

1994). Although no contractional kink bands were observed in conjugate relations the experimentally derived relationships between ϕ and α, ϕ and β, and ϕ and ψ (Gay and Weiss, 1974; Figure 18 & Table 5) have been used to estimate values of ϕ and therefore ε_z. The angles of ϕ determined for sinistral and dextral kink bands (Table 5) display a level of consistency rarely reported in natural systems (c.f. Figure 11 in Goscombe *et al*., 1994). The geometry of sinistral kink bands indicates a shortening direction of 010°, whilst the geometry of the dextral kink bands indicates a shortening direction of 335°. Because no contractional kink bands were observed in conjugate relations and no cross cutting relationships observed, the differences in the principal shortening directions determined from sinistral and dextral kink bands may have several implications:

1. The sinistral and dextral kink bands formed in response to two separate periods of deformation (D_4 & D_5? See Section A).
2. Localised variations in the strain field existed during kink band nucleation and growth.
3. The geometry and relative intensity of the four sets of D_3 extensional kink bands, at any given location, was a fundamental control on the geometry and orientation of contractional kink bands.

A late period of ~N-S shortening characterised by an E-W striking foliation at Ballarat and a NE-SW foliation at Bendigo, St. Arnaud and Inglewood has been recognised by Forde (1989). Within the Stawell Zone (Wilson *et al*., 1992; Miller *et al*., 2001; Miller & Wilson 2002; Miller & Wilson, 2004) the formation of major sets of oblique faults has been attributed to a NW-SE shortening event ('early South Fault' structures) and subsequent NE-SW shortening event ('South Fault-age' structures). NE and ENE trending cleavages are thought to be related to the NW-SE shortening event (Miller & Wilson, 2004). Gray & Willman (1991c) concluded that the fault zones in the eastern BZ are characterised by a weak to intense NW trending crenulation cleavage that is locally overprinted by a weakly developed NE trending crenulation cleavage. Gray & Willman (1991c) relate the two overprinting crenulation cleavages to strike-slip reactivation of fault zones, with initial dextral movement followed by a weaker sinistral movement. It is suggested that the dextral movement is associated with the Tabberabberan Orogeny (*ca.* 381-377 Ma) and that the later sinistral movement might possibly relate to the Middle Carboniferous Kanimblan Orogeny (*ca.* 360-340 Ma; Gray

& Willman, 1991c). Morand *et al*. (1997) suggest that a weak NW trending cleavage exists throughout much of the Melbourne Zone and is related to a NE-SW compressional event that may represent the latest stages of the Tabberabberan Orogeny. VandenBerg *et al*. (2000) propose that the eastern part of the BZ (Figure 1b, c) was affected by a period of N-S shortening late in the Tabberabberan Orogeny. Dextral movement along the Heathcote Fault Zone (Figure 1c) and other smaller faults, the formation of E to NE trending megakinks (e.g. the Tooborac Megakink) and a NW trending cleavage are associated with this shortening event (VandenBerg *et al*., 2000).

A period of N-S to NNE-SSW shortening is proposed from the study of contractional kink bands and mega-kinks located within the Eastern Sub-province of the LFB (Figure 1b; Powell *et al*., 1985; Stubley, 1990). Powell *et al*. (1985) hypothesise that the formation of the kink bands involved a continent-wide stress field and that the N-S shortening experienced in the eastern LFB was related to the Carboniferous Alice Springs Orogeny. Goscombe *et al*. (1994) propose a principal shortening direction of 166º based on the geometry of cm- to kilometre-scale contractional kink bands located within the Mathinna Group, northeast Tasmania. Goscombe *et al*. (1994) suggest that these kink bands are comparable to the kink bands observed by Powell *et al*. (1985).

For a single set of contractional kink bands ε_z normally lies within the acute angle defined by the external foliation and the axial plane (e.g. Gay & Weiss, 1974, p. 290-292). On this basis it is suggested that the dextral and sinistral contractional kink bands recognised in this study formed in response to two separate periods of deformation. In context with the work of others it is proposed that the NE striking sinistral kink bands formed first and in response to a N-S to NNE-SSW shortening event. The sinistral kink bands may be comparable to the NE-SW trending foliation of Forde (1991), the E to NE trending megakinks and NW trending cleavage of VandenBerg *et al*. (2000), the weak NW trending cleavage of Morand *et al*. (1997), the NW trending crenulation cleavage of Gray & Willman (1991c) and the 'South Fault-age' structures of Miller & Wilson (2004). The timing of the sinistral contractional kink bands is thought to correspond to the later stages of the Tabberabberan Orogeny. The W to WNW striking dextral kink bands recognised by this study formed in response to NNW directed shortening. It is suggested that the dextral kink bands are comparable to the NE trending crenulation cleavage of Gray & Willman (1991c) and the contractional kink bands of Powell *et al*. (1985), Stubley (1990) and Goscombe *et al*. (1994). The timing of deformation and kink

band growth may be Carboniferous in age (c.f. Gray & Willman, 1991c; Powell *et al*., 1985).

CONCLUSIONS

1. Four sets of synchronous extensional kink bands arranged in approximately orthorhombic symmetry about a sub-vertical axis have been recognised in kink bands for the first time.

2. The orthorhombic symmetry displayed by the four sets of kink bands appears to be similar to the fault systems reported by Aydin & Reches (1982) and Krantz (1988). However, it was not possible to define the principal strain axes using the 'odd axis' model of Krantz (1988).

3. The extensional kink bands appear to have formed from a kinking mechanism similar to that of the constant-segment-length model (Anderson, 1964; Dewey, 1965; Donath, 1968), with extension and further rotation of the internal foliation occurring only after the internal foliation had been rotated to some limiting angle.

4. The simplified geometric properties of the kilometre-scale kink bands imply that they possess extensional geometry and are comparable to the mm-scale extensional kink bands observed in thin section. This supports the relative timing of kink band formation as suggested in Section A. It is also proposed that the kilometre-scale extensional kink bands contribute significantly to the architecture of the goldfield.

5. The angles of ϕ (Figure 4a) determined for sinistral and dextral contractional kink bands (Table 5) display a level of consistency rarely reported of natural systems. It is suggested that the consistency reflects the systematic manor in which the kink bands were investigated, in particular, the use of true angles as a posed to apparent angle (e.g. Figures 3a, b & 10). The angles of ϕ also suggest that the sinistral and dextral contractional kink bands formed in response to two separate deformation events (D_4 & D_5).

6. Extensional and contractional kink bands demonstrate substantial variability in apparent α, β and ψ angles, even between consecutive thin sections from a suite (e.g. sections orientated at 20/084 & 40/084). This is an important observation

because it may have significant ramifications for studies that investigate kink bands exposed in outcrop. It is suggested that some of the variability associated with naturally occurring kink band systems, as documented by previous authors, is related to the plane in which the kink bands are studied.

7. Comparisons made between principal shortening directions inferred from naturally occurring kink bands and experimentally derived relationships frequently reveal inconsistencies (e.g. Dewey, 1965; Anderson, 1968; Stubley, 1990; Goscombe *et al*., 1994). It can be assumed that the experimental data were obtained from a plane orthogonal to the kink band axial surfaces. Therefore it is highly likely that discrepancies will exist if naturally occurring kink bands are studied in a plane that is not orthogonal to the kink band axial surfaces (see point 5 above). The 'conjugate bisector' method of Ramsay (1962) could be affected in a similar way. An asymmetry of conjugate kink bands could be in part, related to the plane in which they are viewed. This study has highlighted that caution needs to be taken to differentiate between apparent and true angles when investigating the geometry of kink bands.

SECTION C